THE JOURNAL OF COMPARATIVE NEUROLOGY 500:973–1006 (2007)

Cytoarchitectonic and Chemoarchitectonic Subdivisions of the Perirhinal and Parahippocampal Cortices in Macaque Monkeys

KADHARBATCHA S. SALEEM,[1,2]* JOSEPH L. PRICE,[2] AND TSUTOMU HASHIKAWA[1]
[1]Riken Brain Science Institute, Saitama 351-0198, Japan
[2]Department of Anatomy and Neurobiology, Washington University School of Medicine, St. Louis, Missouri 63110

ABSTRACT

Although the perirhinal and parahippocampal cortices have been shown to be critically involved in memory processing, the boundaries and extent of these areas have been controversial. To produce a more objective and reproducible description, the architectonic boundaries and structure of the perirhinal (areas 35 and 36) and parahippocampal (areas TF and TH) cortices were analyzed in three macaque species, with four different staining methods [Nissl and immunohistochemistry for parvalbumin, nonphosphorylated neurofilaments (with SMI-32), and the m2 muscarinic acetylcholine receptor]. We further correlated the architectonic boundary of the parahippocampal cortex with connections to and from different subregions of anterior area TE and with previously published connections with the prefrontal cortex and temporal pole (Kondo et al. [2005] J. Comp. Neurol. 493:479–509). Together, these data provided a clear delineation of the perirhinal and parahippocampal areas, although it differs from previous descriptions. In particular, we did not extend the perirhinal cortex into the temporal pole, and the lateral boundaries of areas 36 and TF with area TE were placed more medially than in other studies. The lateral boundary of area TF in *Macaca fuscata* was located more laterally than in *Macaca fascicularis* or *Macaca mulatta*, although there was no difference in architectonic structure. We recognized a caudal, granular part of the parahippocampal cortex that we termed "area TFO." This area closely resembles the laterally adjacent area TE and the caudally adjacent area V4 but is clearly different from the more rostral area TF. These areas are likely to have distinct functions. J. Comp. Neurol. 500: 973–1006, 2007.

Indexing terms: inferotemporal area TE; areas 35/36; areas TF/TH; area 28; temporal pole; parvalbumin; SMI-32

In the past decade, a great deal of interest has developed in the functions and neuroanatomical organization of the perirhinal (areas 35 and 36) and parahippocampal (areas TF and TH) cortical areas in macaque monkeys. Several behavioral studies have shown that lesions of the perirhinal cortex, with or without damage to the parahippocampal cortex or entorhinal cortex (area 28), produce significant deficits in visual recognition memory (Zola-Morgan et al., 1989; Gaffan and Murray, 1992; Meunier et al., 1993; Suzuki et al., 1993; Buckley et al., 1997; Buckley and Gaffan, 1997; Murray and Bussey, 1999; Murray and Richmond, 2001; Hadfield et al., 2003; Alvarado and Bachevalier, 2005). Indeed, these deficits are possibly even greater than the deficits produced by restricted lesions to the hippocampus (Murray and Bussey, 1999; Baxter and Murray, 2001). Damage to areas TF and TH produces only a mild effect on the visual recognition memory tasks, but such lesions cause deficits in spatial memory

Grant sponsor: Riken Brain Science Institute; Grant sponsor: National Institutes of Health; Grant number: MH70941.

*Correspondence to: K.S. Saleem, PhD, Department of Anatomy and Neurobiology, Washington University School of Medicine, 660 S. Euclid Avenue, St. Louis, MO 63110. E-mail: saleemk@wustl.edu

Received 22 March 2006; Revised 5 June 2006; Accepted 13 July 2006
DOI 10.1002/cne.21141
Published online in Wiley InterScience (www.interscience.wiley.com).

tasks or object-place association tasks (Malkova and Mishkin, 2003; Alvarado and Bachevalier, 2005).

Several anatomical investigations in primates have indicated that the perirhinal and parahippocampal cortices receive afferent projections from areas in the temporal, parietal, and frontal cortices (Van Hoesen and Pandya, 1975a; Van Hoesen et al., 1975; Seltzer and Pandya, 1976; Martin-Elkins and Horel, 1992; Suzuki and Amaral, 1994a; Saleem and Tanaka, 1996; Blatt et al., 2003; Kondo et al., 2005). In turn, the perirhinal and parahippocampal cortices send efferent projections to hippocampus directly or indirectly via the entorhinal cortex (Van Hoesen and Pandya, 1975b; Witter et al., 1989; Witter and Amaral, 1991; Suzuki and Amaral, 1994b; Yukie, 2000). Thus both of these cortical areas serve the role of connecting the neocortex with the hippocampus.

In spite of the significance of the perirhinal and parahippocampal cortices, their anatomical organization, rostrocaudal and mediolateral extent, and architectonic boundaries with adjacent cortical areas have been controversial. This is significant, because the connections and functions that are ascribed to the perirhinal and parahippocampal cortices depend critically on how the boundaries of the areas are drawn. If boundaries are drawn to include a larger, heterogeneous area, the properties of the area will necessarily be less precisely determined.

Early studies by Brodmann (1909) and Van Hoesen and Pandya (1975a) indicated that the perirhinal cortex is a small strip of cortex located in the lateral bank of the rhinal sulcus in rhesus monkeys (*M. mulatta*). However, Amaral and his colleagues (Amaral et al., 1987; Insausti et al., 1987; Suzuki and Amaral, 1994a; Stefanacci et al., 1996; Lavenex et al., 2002), based on anatomical connections and architectonic studies, extended the perirhinal cortex laterally to include a substantial part of the inferior temporal gyrus and rostrally to include parts of the dorsal and ventral temporal pole (see also Munoz and Insausti, 2005). Over the same time period, other cytoarchitectonic and/or connectional studies defined a less extensive perirhinal cortex (Saleem and Tanaka, 1996; Blatt and Rosene, 1998; Yukie, 2000) and recognized the temporal pole as a distinct architectonic region (Markowitsch et al., 1985; Moran et al., 1987; Gower, 1989; Seltzer and Pandya, 1989; Kondo et al., 2003).

The architectonic boundaries of the parahippocampal cortex (areas TF and TH) have also been inconsistent across different studies (Seltzer and Pandya, 1976; Blatt and Rosene, 1998; Yukie, 2000; Suzuki and Amaral, 2003; Blatt et al., 2003). In addition, there may be differences between subspecies of macaque monkeys. For example, for *M. fascicularis* (cynomolgous monkey), Suzuki and Amaral (2003) placed the lateral boundary of area TF with area TE at the medial lip of the occipitotemporal sulcus (ots) and medial to the anterior middle temporal sulcus (their Fig. 15). In contrast, other investigators described this boundary in the fundus or the lateral bank of the ots in *M. fuscata* and *M. mulatta* (Japanese monkey and rhesus monkey, respectively; Yukie, 2000; Blatt et al., 2003). These species differences have not yet been examined systematically, but they are comparable to differences seen in other parts of the cortex. In the auditory cortex, species differences in the size and relative positions of the core and belt areas have been reported between *M. fuscata* and *M. fascicularis* (Jones et al., 1995). A more subtle difference in the cytoarchitectonic organization of the entorhinal cortex (area 28) has also been shown between two allopatric species, *M. fascicularis* and *M. mulatta* (Van Hoesen and Pandya, 1975a; Amaral et al., 1987).

In the present investigation, we used cytoarchitectonic and chemoarchitectonic analyses to reexamine the spatial extent, subdivisions, and boundaries of the perirhinal and parahippocampal cortices and the adjacent inferotemporal area TE in macaque monkeys. In addition to the standard Nissl method, we used immunohistochemical stains for the calcium-binding protein parvalbumin, a nonphosphorylated epitope of the neurofilament protein (recognized by the SMI-32 antibody), and the m2 muscarinic acetylcholine receptor (m2-AChR), each of which provides very useful distinctions in the medial temporal cortex. This use of several staining methods has allowed more objective

Abbreviations

28	entorhinal cortex
28Ll	lateral entorhinal cortex, lateral subregion
28Lm	lateral entorhinal cortex, medial subregion
35	area 35 of the perirhinal cortex
36c	area 36 of the perirhinal cortex, caudal subregion
36p	area 36 of the perirhinal cortex, temporal-polar subregion
36r	area 36 of the perirhinal cortex, rostral subregion
AI	Primary auditory cortex (core region)
amts	anterior middle temporal sulcus
amy	amygdala
C	caudal
CA1	CA1 subfield of the hippocampus
cs or cas	calcarine sulcus
H	hypothalamus
HC	hippocampus
L	lateral
LD	lamina dissecans
LGN	lateral geniculate nucleus
ls	lateral sulcus
M	medial
MDmc	mediodorsal thalamus, magnocellular subregion
MDpc	mediodorsal thalamus, parvicellular subregion
MGN	medial geniculate nucleus
ots	occipitotemporal sulcus
p-amy	periamygdaloid cortex
PI	inferior pulvinar
PL	lateral pulvinar
PM	medial pulvinar
R	rostral
rs	rhinal sulcus
RTp	rostrotemporal part of the auditory cortex, polar subdivision
SI	primary somatosensory cortex
SII	secondary somatosensory cortex
STGr	superior temporal gyrus, rostral part
sts	superior temporal sulcus
TEad	dorsal subregion of anterior TE
TEav	ventral subregion of anterior TE
TEO	area TEO
TEpd	dorsal subregion of posterior TE
TEpv	ventral subregion of posterior TE
TF	area TF of the parahippocampal cortex
TFO	area TFO of the parahippocampal cortex
TGa	agranular part of the temporal pole
TGdd	dysgranular part of the dorsal temporal pole
TGvd	dysgranular part of the ventral temporal pole
TH	area TH of the parahippocampal cortex
V4	visual area 4
WM	white matter

and reproducible definition of the extent and boundaries of areas in the medial temporal lobe. Although other stains (e.g., acetylcholinesterase and calbindin) may also be useful for other regions such as the prefrontal cortex (Carmichael and Price, 1994), these are less useful for the perirhinal and parahippocampal areas. We also described briefly the architectonic organization of the lateral part of the entorhinal cortex (area 28) within the rhinal sulcus, to define better its boundary with the perirhinal cortex. We analyzed three different species of macaque monkeys: *M. fascicularis*, *M. fuscata*, and *M. mulatta*. The dorsal and ventral subregions of the temporal pole were also described, to clarify whether these subregions of the temporal pole (area TG; von Bonin and Bailey, 1947) are part of the perirhinal cortex. Finally, we made axonal tracer [wheat germ agglutinin-horseradish peroxidase (WGA-HRP)] injections into dorsal and ventral subregions of anterior TE (TEad and TEav, respectively) in both *M. fascicularis* and *M. fuscata*, to determine the origin and extent of projections to those areas from the medial temporal cortex. These were correlated with the results of a previous study on the connections of the perirhinal and parahippocampal cortices with the prefrontal cortex (Kondo et al., 2005). These connectional analyses were particularly useful for the demarcation of the rostral boundary of area TF with the entorhinal cortex and the lateral boundary of TF with the posterior ventral TE (TEpv).

MATERIALS AND METHODS

Three adult cynomolgous monkeys (*Macaca fascicularis*) and two rhesus monkeys (*Macaca mulatta*) were used in this study. In two cynomolgous monkeys, WGA-HRP was injected into area TEad or TEav, to examine the spatial extent of labeled neurons and terminals in and around the parahippocampal cortex (areas TF and TH). The remaining cynomolgous monkey and two rhesus monkeys brains were processed for immunohistochemical methods; these cases did not receive tracer injections in the temporal cortex. In addition, a number of Japanese monkeys (*M. fuscata*) and cynomolgous monkeys that had been prepared and used in previous studies (Carmichael and Price, 1994; Saleem and Tanaka, 1996; Saleem et al., 2000; Kondo et al., 2003, Kondo et al., 2005) were reexamined and reanalyzed in relation to the architectonic organization of perirhinal and parahippocampal cortices. The Japanese monkeys also had WGA-HRP injections in area TEad or TEav, which demonstrated connections with areas TF and TH.

Surgery and tracer injection

The tracers were injected during aseptic surgery under general anesthesia, as described previously (Saleem and Tanaka, 1996; Saleem et al., 2000). After pretreatment with atropine sulfate (0.1 mg/kg, i.m.) and sedation with ketamine hydrochloride (12 mg/kg, i.m.), each monkey was anesthetized by intraperitoneal injection of sodium pentobarbital (35 mg/kg). Supplemental doses of sodium pentobarbital (9 mg/kg, i.p.) were given as needed to maintain a surgical level of anesthesia. Tranexamic acid (25 mg/kg, i.m.) was given to minimize bleeding. The body temperature, heart rate, and respiratory rate were monitored throughout surgery. The experimental protocol had been approved by the Experimental Animal Committee of the RIKEN Institute and conformed to the NIH guidelines.

Once anesthesia was established, the animals were placed in a stereotaxic apparatus, and the scalp was incised. The superior temporal sulcus and the anterior middle temporal sulcus (amts) were exposed after craniotomy to determine the injection site. WGA-HRP (5%, Toyobo, Japan) was injected by pressure, according to the method described by Saleem and Tanaka (1996). The tracer was injected into a single site in TEad or TEav (0.1 μl), except in one *M. fascicularis* case, in which WGA-HRP was injected in four sites (0.1 μl/site), to cover a larger part of TEad (see Fig. 21A). After the injection was completed, the dura was sutured and the wound was closed. Dexamethasone sodium phosphate (1 mg/kg i.m.) was given after the surgery to minimize cerebral edema. The antibiotic piperacillin sodium (55 mg/kg, i.m.) and analgesic ketoprofen (5 mg/kg, i.m.) were injected after surgery.

Histological processing

Two days following the WGA-HRP injection, the operated monkeys were deeply anesthetized with a lethal dose of sodium pentobarbital (60–80 mg/kg, i.v.) and perfused transcardially with 1 liter of 0.9% warm heparinized NaCl, followed by 3–4 liters of cold 4% paraformaldehyde in 0.1 M phosphate buffer (PB; pH 7.2–7.4), 1–2 liters of 10% sucrose in 0.1 M PB, and finally 1 liter of 20% sucrose in 0.1 M PB. The flow rate of the fixative solution was adjusted so that the perfusion with paraformaldehyde took 30–45 minutes. The brain was immediately removed from the skull, carefully blocked in the stereotaxic plane, photographed, and then stored in 30% buffered sucrose at 4°C until it sank. Frozen sections were cut in the coronal plane at 50-μm thickness. A series of every fifth section (250-μm interval) was processed for the HRP histochemistry. The HRP reaction was carried out according to the modified tetramethyl benzidine method described by Gibson et al. (1984). The adjacent series of sections was stained for Nissl or immunohistochemically with antibodies against parvalbumin and a nonphosphorylated epitope of neurofilaments (SMI-32; see below for details).

The unoperated animals were deeply anesthetized with ketamine hydrochloride (12 mg/kg, i.m.) and sodium pentobarbital (60–80 mg/kg, i.v.) and perfused transcardially either with paraformaldehyde, as described above with slight modifications for immunocytochemistry, or with a pH shift fixation method as described by Pitkanen and Amaral (1991), with some modifications. In the first method, the animals were prefused with 0.9% warm heparinized NaCl followed by the 1 liter of 1% paraformaldehyde in 0.1 M PB (pH 7.4, 4°C) for 10 minutes, 2 liters of 4% paraformaldehyde in 0.1 M PB (pH 7.4, 4°C) for 20 minutes and finally 1 liter of 4% paraformaldehyde and 10% sucrose in 0.1 M PB (pH 7.4, 4°C) for 15 minutes. In the pH shift fixation, the animal was perfused transcardially with 1 liter of 0.9% warm heparinized NaCl, followed by 1 liter of 4% paraformaldehyde in 0.1 M sodium acetate buffer (pH 6.5, 4°C), then 2 liters of 4% paraformaldehyde in 0.1 M sodium borate buffer (pH 9.5, 4°C), and finally 1 liter of 4% paraformaldehyde and 10% sucrose in 0.1 M sodium borate buffer.

In these cases, the brains were then removed, photographed, carefully blocked in the stereotaxic plane, and postfixed for 6 hours in the final fixative-sucrose solution,

TABLE 1. Antibodies Used

Antibody	Source	Catalog No.	Type	Immunogen	Species	Dilution
Parvalbumin	Sigma	P-3171, clone PA-235	Monoclonal IgG1	Parvalbumin from carp muscle	Mouse	1:2,000
SMI-32	Sternberger Monoclonals	SMI-32	Monoclonal IgG1	Neurofilament heavy chain (nonphosphorylated)	Mouse	1:2,000 or 1:5,000
m2-AChR	Chemicon	MAB367	Monoclonal IgG2a	i3 Loop of m2 receptor fusion protein (225-359), fused to glutathione S-transferase (GST)	Rat	1:2,000

then stored in 20% and 30% sucrose in 0.1 M PB at 4°C until they sank. Frozen sections were cut in the coronal plane at 40 or 50 μm thickness. An adjacent series of every fifth section was stained for Nissl or immunohistochemically for parvalbumin, the nonphosphorylated neurofilament protein (SMI-32), and the m2 muscarinic acetylcholine receptor (m2-AChR).

Immunohistochemical procedures

Details of the antibodies used are given in Table 1. The parvalbumin antibody was raised against parvalbumin from carp muscle. It was determined to be specific by immunoblotting (Western blot) and to stain specifically the 12,000-molecular-weight band that was identified as parvalbumin by Ca binding (Sigma data sheet). The SMI-32 antibody recognizes a nonphosphorylated epitope of neurofilament H. It was shown to be specific by immunoblot, where it recognizes a double band at MW 200,000 and 180,000, which merge into a single neurofilament H line on two-dimensional blots (Sternberger and Sternberger, 1983; Goldstein et al., 1987). The antibody has been shown to stain a subpopulation of pyramidal cells in the neocortex (see, e.g., Campbell and Morrison, 1989; Hof and Morrison, 1995); the pattern of staining seen in this study corresponds to well-established patterns from many previous studies. The antibody against the m2-AChR was raised against the i3 loop of the receptor. It was shown to recognize a single band on Western blots corresponding to the m2i3-GST fusion protein (Levey et al., 1995); in immunohistochemical stains, it was also shown to demonstrate a pattern identical to that seen previously with polyclonal antibodies against the same antigen (Levey et al., 1991, Levey et al., 1995).

Free-floating sections were preincubated in the phosphate-buffered saline (PBS), containing 0.5% Triton X-100 and 5% normal serum (normal horse serum for parvalbumin and SMI-32 or normal goat serum for m2-AChR) and 2% bovine serum albumin (BSA) for 60 minutes at room temperature. The sections were then incubated in PBS containing 0.3% Triton X-100, 3% normal serum, 1% BSA, and the primary antibody for 2 days at 4°C. After washing with PBS, sections were incubated in PBS containing 0.3% Triton X-100, normal serum, 0.5% BSA, and the biotinylated horse antimouse IgG (for parvalbumin and SMI-32) or biotinylated goat antirat IgG (m2-AChR) for 90 minutes at room temperature. After washing with PBS, sections were developed in a solution containing 0.05 M Tris buffer (pH 7.2–7.4), 0.05% diaminobenzidine (DAB), and 0.003% H_2O_2. The sections were then mounted on glass slides, air dried, dehydrated, and coverslipped with Entellan or DPX. In some cases, the immunostaining was intensified by serial immersions in 0.005% osmium tetroxide, 0.5% thiocarbohydrizide, and 0.005% osmium tetroxide before mounting.

Data analysis

The sections were observed with a light microscope under bright- and darkfield illumination. Photographs were taken with a CCD camera attached to the microscope and processed in Adobe Photoshop. In the WGA-HRP cases, the distribution of labeled terminals and retrogradely labeled cell bodies in the parahippocampal gyrus, perirhinal cortex, and areas TEad, TEav, TEpd, and TEpv were plotted onto enlarged camera lucida drawings of sections at ×100 magnification. Sections were usually sampled at 0.5–1-mm intervals.

Sections stained for parvalbumin were analyzed further in two ways. First, sections were scanned by a MapAnalyser Densitometry System (Yamato Scientific Co., Tokyo, Japan). The entire area of the histology section was scanned at 50-μm steps with a field diaphragm at 25-μm in diameter (photomultiplier voltage, 400 V; objective, ×20; for other details see Ichinohe and Rockland, 2005a). A large part of the temporal lobe was scanned in a series of sections, including the temporal pole; the superior temporal sulcus (sts); inferotemporal cortex (area TE); the entorhinal, perirhinal and parahippocampal cortices; the amygdala; and the hippocampus. Denser immunostaining, corresponding primarily to fiber staining, was coded as red and less dense staining as blue (Fig. 1).

In addition, the spatial and laminar distribution patterns of parvalbumin-stained neurons were examined in the perirhinal and parahippocampal cortices and adjacent areas TE and entorhinal cortex. In each subregion, the location of all immunolabeled cell bodies in a 500-μm-wide traverse from the pial surface through the entire depth of the cortex was plotted at a magnification of ×100 with the aid of a camera lucida. Each traverse was subdivided into 50-μm-deep horizontal bins and was plotted in a histogram as a function of cortical depth (e.g., see Fig. 7).

Finally, MRI scans (3T scanner; T1 MPRAGE image with 0.5–0.75-mm voxels) were available for five *Macaca fascicularis* monkeys. These were used to measure the rostrocaudal extent of the perirhinal and parahippocampal cortical areas, based on sulcal landmarks that were defined in histological sections. These measurements were free of histological shrinkage.

RESULTS

The structure and delineation of the perirhinal and parahippocampal cortices will be first described in detail for *M. fascicularis*. After this, the similarities and differences in *M. fuscata* and *M. mulatta* will be described.

Cytoarchitectonic and chemoarchitectonic subdivisions of the perirhinal cortex (areas 35 and 36)

This medial temporal region was initially described for humans by Brodmann (1909), who distinguished area 35

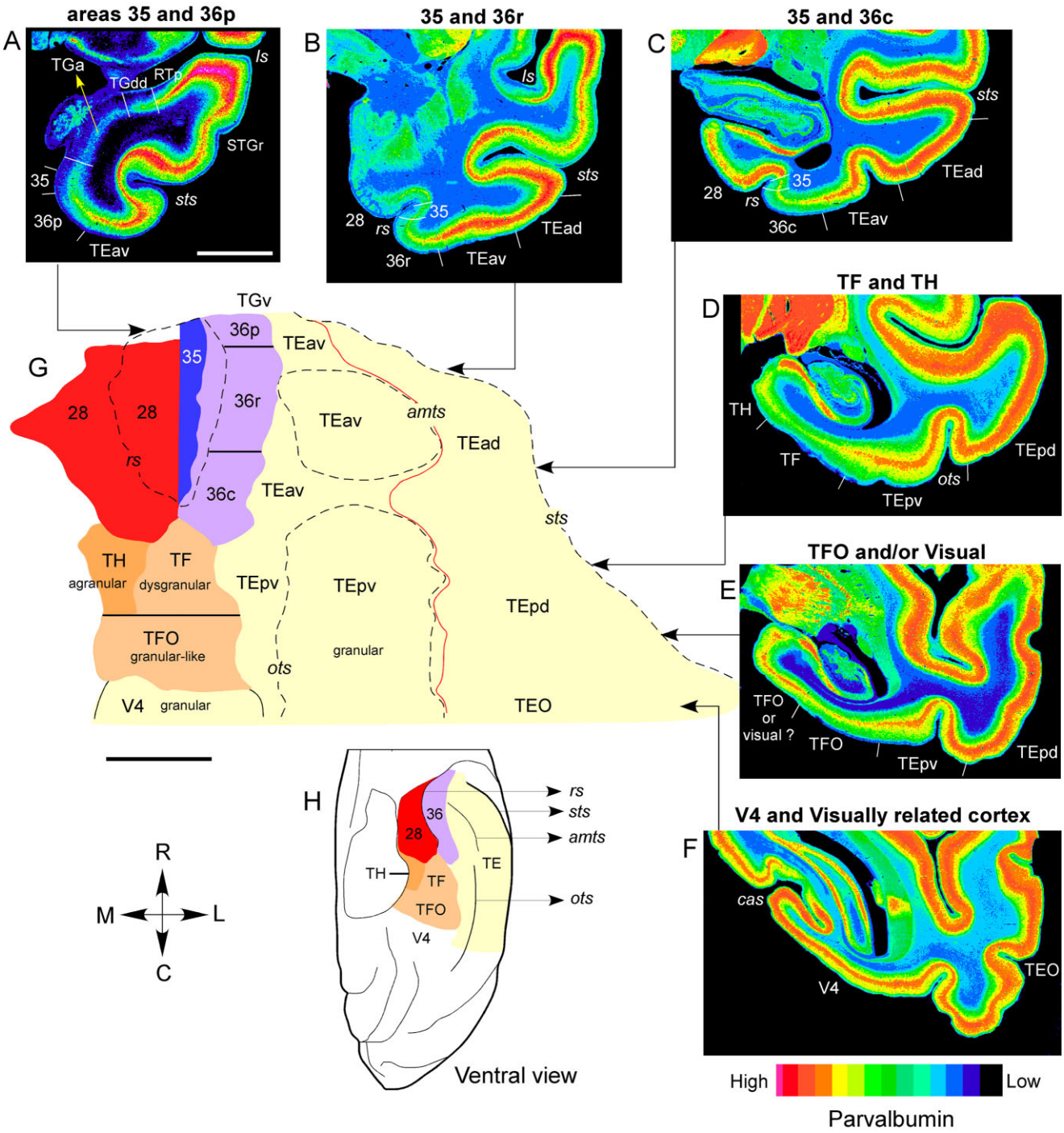

Fig. 1. Chemoarchitectonic subdivisions of the perirhinal and parahippocampal cortices in macaque monkeys. **A–F:** Series of color-coded images of parvalbumin-stained sections through the medial and lateral temporal cortex, including the perirhinal cortex (areas 35 and 36), the parahippocampal cortex (areas TH, TF, and TFO), and areas 28 and TE (and its subdivisions) of a rhesus monkey (*M. mulatta*), made with the "MapAnalyzer densitometry system" (see Materials and Methods). Denser immunostaining, corresponding primarily to neuropil staining (cf. Fig. 6E), was coded as red and weak staining as blue. The white lines normal to the surface mark boundaries between areas. Note that there is a clear decrease in the density of parvalbumin staining in areas 35, 36 (A–C), TF (D), and to a lesser extent TFO (E). **G,H:** Unfolded map and ventral brain surface of a cynomolgous monkey (*M. fascicularis*), illustrating the perirhinal cortex (blue and purple), parahippocampal cortex (light and dark orange), area 28 (red), subdivisions of area TE, and area V4 (both yellow). The overall architectonic organization of perirhinal and parahippocampal cortices in rhesus monkey is similar to that of the cynomolgous monkey. The dashed lines on the map indicate the lips of the sulci (amts, ots, rs, and sts), and the solid lines show the borders between different subdivisions of the perirhinal and parahippocampal cortices. The red line indicates the boundary between dorsal and ventral TE. The solid lines with arrows at the sides of the unfolded map show the approximate location of parvalbumin-stained sections (A–F). Scale bars = 5 mm in A (applies to A–F); 5 mm in G.

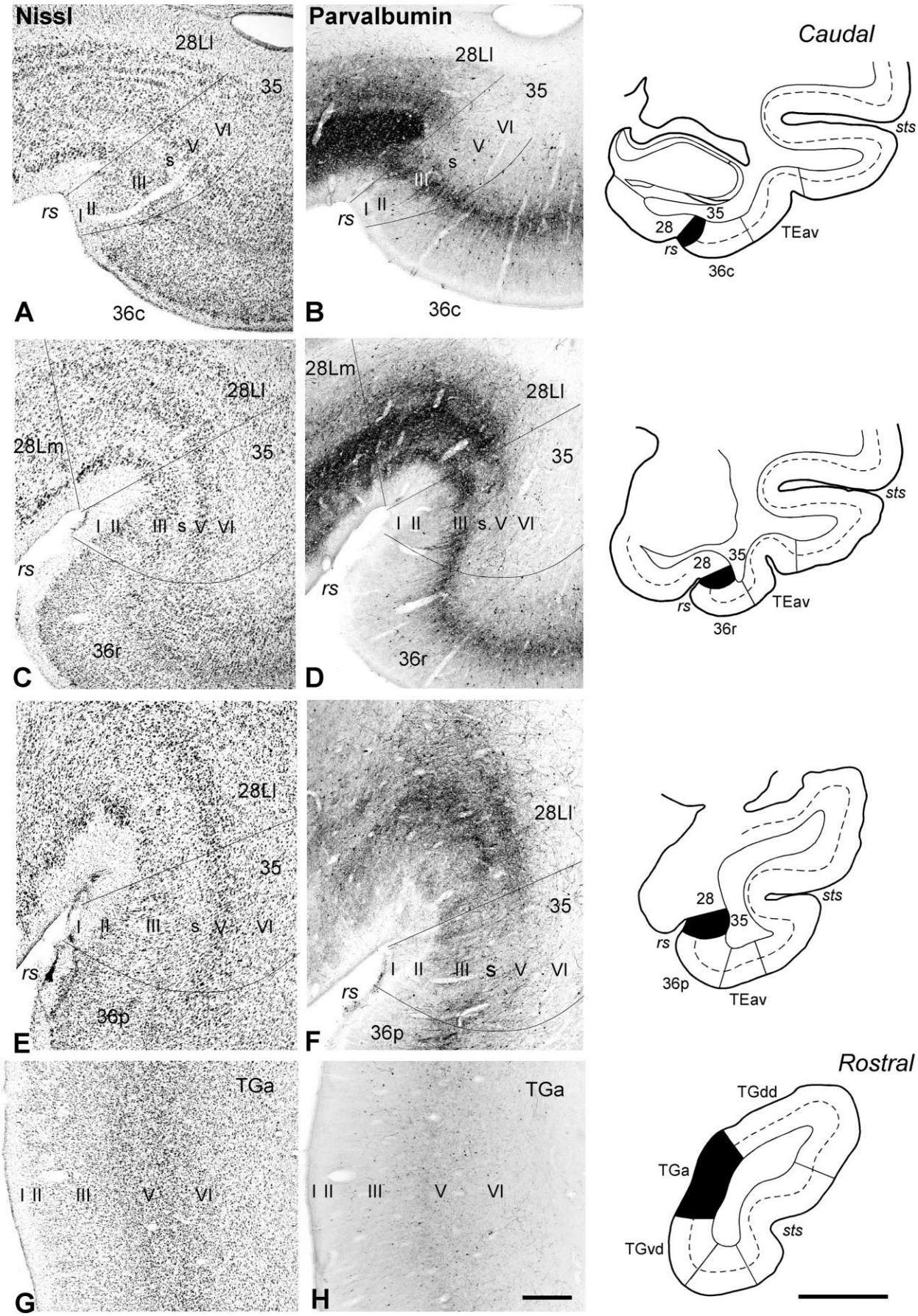
Nissl
Parvalbumin
Caudal
28LI
35
VI
V
s
III
I II
rs
sts
28
TEav
36c
A
B
28Lm
III s V VI
36r
C
D
III s V VI
36p
E
F
TGa
TGdd
TGvd
Rostral
G
H

Figure 2

as perirhinal cortex and area 36 as ectorhinal cortex (see Garey, 1994, his Fig. 86, p 110). For monkeys, Brodmann (1909) did not include either area 35 or area 36 in his map of the cercopithicid monkey (guenon) cortex (see Garey, 1994, his Fig. 91, p 131), although he illustrated a section from a rhesus monkey that shows well-developed areas 35 and 36 (Garey, 1994, his Fig. 26, p 43). More recently, both areas 35 and 36 have been recognized in monkeys, but it has been common to refer to both of them as the "perirhinal cortex," and the term "ectorhinal" has been dropped (Amaral et al., 1987; Insausti et al., 1987; Suzuki and Amaral, 1994a, Suzuki and Amaral, 2003; Saleem and Tanaka, 1996; Yukie, 2000; Kondo et al., 2005).

In the current study, we also refer to both areas 35 and 36 as perirhinal cortex. These are distinct from each other and from the temporal areas lateral to them. There are some variations within the perirhinal areas in the rostrocaudal axis, especially in area 36, but we did not find clear architectonic variation within the mediolateral axis of area 35 or 36.

Lateral to the perirhinal cortex is the inferotemporal cortex area TE. As has previously been done, this area will be divided into four subregions, TEad, TEav, TEpd, and TEpv (Yukie et al., 1990; Saleem and Tanaka, 1996). These areas have distinct connections with each other, the cortex of the sts, the hippocampus, the amygdala, and the entorhinal, perirhinal, and parahippocampal cortices (Yukie et al., 1990; Saleem and Tanaka, 1996; Cheng et al., 1997; Saleem et al., 2000; Yukie, 2000).

Area 35

Area 35 is a narrow strip of cortex (1–1.5 mm wide) located within the lateral fundus and bank of the rhinal sulcus (Fig. 1), between the entorhinal cortex (area 28) medially and area 36 laterally. The border with the entorhinal cortex is especially obvious in sections stained for parvalbumin and the m2-AChR (see below; Figs. 2–4); based on these, the border between area 35 and the entorhinal cortex is at the fundus of the rhinal sulcus caudally (Fig. 2A,B) and moves slightly into the lateral bank of the sulcus rostrally (Fig. 2E,F). The rostral border of area 35 is at the rostral end of the rhinal sulcus, where it is replaced by the agranular temporal pole (area TGa; Kondo et al., 2003; Fig. 2G,H). Caudally, area 35 ends approximately at the caudal end of the rhinal sulcus (Fig. 1G). The full rostrocaudal extent of area 35 is about 6–9 mm, based on measurements of the distance from the rostral to caudal ends of the rhinal sulcus, visualized in magnetic resonance images (MRI) of five *Macaca fascicularis* monkeys.

The lateral part of the entorhinal cortex, area 28L, will be briefly described because it defines the medial border of area 35. Area 28L can be further divided into lateral and medial subregions (28Ll and 28Lm, respectively) in Nissl-, parvalbumin-, and SMI-32-stained sections (Fig. 3, first row). Both subregions correspond to area EL of Amaral et al. (1987), Insausti et al. (1987), and Pitkanen and Amaral (1993) and partially correspond to area 28S of Saunders et al. (1988). The medial subregion (28Lm) is located in the medial bank of rhinal sulcus; it has a relatively less dense layer III, no obvious lamina dissecans (or inner plexiform layer), and less distinct layer V. The lateral subregion (area 28Ll) borders area 35 at the lateral edge of the fundus of rhinal sulcus. It extends roughly 1.5 mm in the mediolateral direction and is strikingly demarcated by a dense band of darkly stained neurons in layer V (Fig. 3A). Although this band of neurons seems to continue laterally from area 28Ll into layer V of area 35, a marked boundary between the two areas is apparent in parvalbumin-stained sections (see below; Fig. 3D). Area 28Ll has moderately strong neuronal and dendritic staining with SMI-32 in layers II and V (Fig. 3G). Area 28Lm is distinguished from areas 28Ll and 35 by its relative lack of staining in layer V (Fig. 3G).

Nissl. In Nissl-stained sections, area 35 is typically characterized by the absence of an internal granular layer (IV) and the presence of a cell-sparse zone between layer III and layer V (Fig. 3A–C). The cell-sparse region (designated as layer "S," for sparse) stands out as a unique layer in area 35 and does not correspond to any layer in area 36 (Figs. 2, 3). Layer II of area 35 is thin and irregular and has slightly smaller and less intensely stained neurons than in area 28 (Fig. 3A,B). Layer III is characterized by a patchy distribution of large and small pyramidal cells, whereas layer S contains only a few small cells (Fig. 3B,F). Layer V consists of pyramidal cells that are similar to those found in layer III but are more densely packed (Fig. 3A,B). Layer VI contains relatively small, sparsely distributed, and lightly stained neurons, with no clear indication of sublamination. In contrast, layer VI of area 28 contains larger cells that are clearly multilaminated, especially in the caudal levels of the cortex (Figs. 2A,C, 3A).

Parvalbumin. Parvalbumin is very effective in specifying structural differences between area 35 and area 28 and other differences among cortical areas in the medial temporal lobe and the inferotemporal cortex (Fig. 1). In particular, a dense plexus of parvalbumin-immunoreactive fibers and terminals in layer V of area 28Ll is largely absent in the contiguous layers S and V of area 35 (Fig. 3D,E). Area 35 is characterized by dense staining of a parvalbumin-immunoreactive plexus in layer III, which shifts into layers II/III in area 28Ll and into layer IV in area 36 (Fig. 3D); this plexus is more prominent in the caudal two-thirds of area 35 (Fig. 2B,D). There are only a few parvalbumin-immunoreactive neurons in layer III of area 35, in contrast to the greater density of immunoreactive neurons in layer IV of area 36 (Fig. 3F).

SMI-32. In area 35, the SMI-32 antibody stains a patchy band of pyramidal neurons and their processes (dendrites) in layer III (Fig. 3G–I). This is particularly distinctive, because area 36 has very few or no immunoreactive neurons and processes in layer III (Fig. 3G). In area 28Ll, there is a similar patchy distribution of neurons and dendrites, but it is in layer II. Layer II of area 35 contains few or no immunoreactive neurons and dendrites

Fig. 2. Photographs of Nissl (**A,C,E**)- and parvalbumin (**B,D,F**)-stained sections, from caudal to rostral, to illustrate the boundaries of area 35 with areas 28 and 36. **G** and **H** also show the contiguous area TGa of the temporal pole. The corresponding line drawings through the temporal lobe in the right column illustrate areas 35 and TGa as solid black regions; the dashed line represents layer IV. The medial border of area 35 with the entorhinal cortex (28Ll) is especially obvious in sections stained for parvalbumin. Note that the parvalbumin-immunoreactive plexus in layer III was more prominent in the caudal and midlevels (B,D) of area 35 than in the rostral part (F). Also note that the cell-sparse layer between layers III and V (layer "S") and the strong parvalbumin staining in layer III of area 35 are absent in area TGa (compare E with G and D with H). Scale bars = 0.5 mm in H (applies to A–H); 5 mm in line drawings.

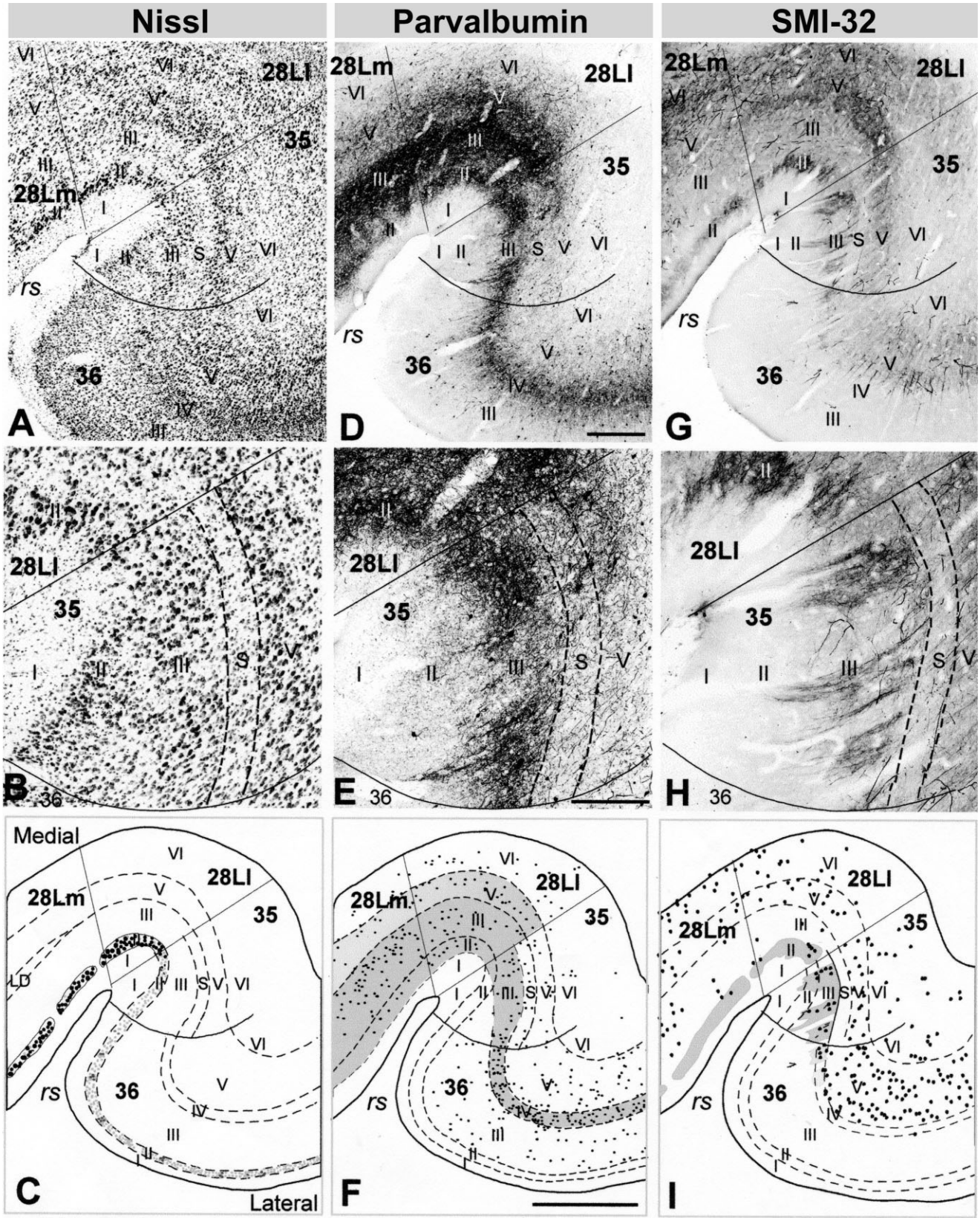

Fig. 3. **A,D,G:** Low-power photomicrographs show the architectonic organization of area 35 and surrounding regions in Nissl-, parvalbumin-, and SMI-32-stained sections. Note that the dense plexus of parvalbumin-immunoreactive fibers and terminals in layer V of area 28 (28Ll) is largely absent in the contiguous layers S and V of area 35 (D). **B,E,H:** High-power photomicrographs of area 35. Note the cell-sparse zone (layer "S") between prominent layers III and V in the Nissl-stained section (B). **C,F,I:** The line drawings detail the laminar pattern in areas 35, 36, and 28, taken from the sections shown in A,D,G. In C, the dots represent the large cells of layer II in area 28, and smaller layer II cells in areas 35 and 36. In F, gray shading indicates the parvalbumin-stained plexus, and dots show the distribution of parvalbumin-stained neurons. In I, gray shading illustrates the patchy distribution of SMI-32-labeled neuronal processes in layer III of area 35 and layer II of area 28, and dots indicate SMI-32-labeled pyramidal neurons. Scale bars = 0.5 mm in D (applies to A,D,G); 0.25 mm in E (applies to B,E,H); 1 mm in F (applies to C,F,I).

(Fig. 3H). Layers S and VI are very lightly stained, but layer V contains a moderate number of stained neurons (Fig. 3G).

This description differs slightly from that of Suzuki and Amaral (2003), who reported that the SMI-32-labeled cell bodies and processes were in layer II of area 35. The disagreement may be due to different placement of the boundary between area 35 and the entorhinal cortex. With the boundary between area 35 and the entorhinal cortex based on staining for parvalbumin and m2-AChR, as in the present study, SMI-32-stained neurons and dendrites are found in layer II in the lateral entorhinal cortex but in layer III in area 35 (Fig. 3G).

m2-AChR. The m2-AChR antibody recognizes a dense fiber and terminal plexus in layer III of the entorhinal cortex, similar to that described by Mash et al. (Mash et al. 1988; in their prorhinal cortex) and Flynn and Mash (1993). This plexus provides a sharp delineation from area 35, which has very weak immunoreactive labeling for m2-AChR (Fig. 4A,B). The border between area 35 and area 28 based on this staining agrees well with the location of the border seen in the Nissl-, parvalbumin-, and SMI-32-stained sections. In area 28, the distribution of m2-immunoreactive labeling in layer III is heterogeneous. The staining is strongest at the lateral edge of the entorhinal cortex (28Ll), and it becomes gradually weaker toward the medial part of the entorhinal cortex (Fig. 4A).

m2-AChR immunoreactivity in other areas. Although unrelated to the present study, it is interesting to note that the dark band of m2-AChR-immunoreactive labeling in the middle cortical layer is observed in other cortical areas that are primarily sensory in function, including the primary somatosensory area SI, primary auditory cortex in the supratemporal plane (A1), and primary visual cortex (V1; Fig. 4C–F; see also Mash et al., 1988; Flynn and Mash, 1993). Substantial m2-AChR immunoreactivity was also observed in some specific subcortical areas: the medial, lateral, and inferior pulvinar; the medial geniculate nucleus; the parvicellular subdivision of the medial dorsal thalamus (MDpc); the superior colliculus; and the lateral hypothalamus (Fig. 4C–F).

Distinction between area 35 and temporal pole

Area 35 is replaced rostrally by the agranular part of the temporal pole (area TGa; Fig. 2), approximately at the rostral end of the rhinal sulcus. Area TGa is a small region (around 1.0–1.5 mm rostrocaudal extent), located between the dorsal and the ventral dysgranular temporal pole areas (TGdd and TGvd, respectively). Caudally it slightly overlaps the most rostral subdivision of the periamygdaloid cortex (PACo; Carmichael et al., 1994). Although both areas 35 and TGa are agranular, their cytoarchitectonic and chemoarchitectonic features are clearly different (Fig. 2G,H). In area TGa, the cell-sparse layer between layers III and V (layer "S" in area 35) is absent. Layers II and III of area TGa contain very sparse immunoreactive neurons and their processes in parvalbumin- and SMI-32-stained sections. In contrast, layer III of area 35 is characterized by dense staining of parvalbumin-immunoreactive fibers and terminals and by SMI-32-immunoreactive pyramidal neurons and their processes (Figs. 2, 3). Layers V and VI are also more poorly differentiated in area TGa than in area 35.

Area 36

Area 36 is a dysgranular or weakly granular cortex situated between area 35 medially and area TEav laterally (Fig. 1). Rostrally, area 36 extends about 2 mm in front of the limen insula (temporal-frontal junction), where it is replaced by area TGvd in the temporal pole. Caudally, area 36 continues about 1–2 mm behind the end of the rhinal sulcus, where it is replaced by the parahippocampal cortex (area TF; Fig. 1G). Area TF first appears between the caudal ends of the entorhinal and perirhinal cortices and then expands to replace both the perirhinal and the entorhinal cortices. Based on measurements from MR images in five *Macaca fascicularis* monkeys, using the sulcal landmarks defined above, area 36 extends for about 11 mm in the rostrocaudal direction.

Rostrocaudal differences in the architectonic characteristics of area 36, together with previous connectional studies (Saleem and Tanaka, 1996; Saleem et al., 2000), prompted us to subdivide area 36 into three subregions caudorostrally. They are areas 36c, 36r, and 36p (caudal, rostral, and temporal-polar subregions of area 36, respectively; Fig. 5). The borders between these subdivisions of area 36 were less clear than the borders of area 36 with surrounding regions. We did not recognize mediolateral subdivisions within area 36 (cf. Suzuki and Amaral, 2003).

Areas 36c and 36r occupy the medial temporal cortex from the caudal part of the rhinal sulcus to the limen insula. Area 36p extends about 1.5–2 mm rostral to the limen insula and is contiguous with the ventromedial, dysgranular temporal pole (TGvd; Kondo et al., 2003). It should be noted that, in our description, the perirhinal cortex does not extend into the dorsal part of the temporal pole (see below).

Area 36c (caudal subregion of area 36)

Nissl. In the Nissl-stained sections; area 36c is the most granular part of area 36. It is further characterized by the presence of prominent pyramidal cells in layer V and the superficial part of layer VI (VIa; Fig. 5A). Layer II is relatively dense and patchy and contains round and pyramidal cells with sparsely distributed glial cells. These architectonic characteristics are mostly absent in the laterally adjacent area TEav at this caudal level. Layer III contains small to large pyramidal neurons with no clear indication of sublamination. Layer IV is distinct but contains fewer granule cells than area TEav. Layer V contains medium-sized to large pyramidal neurons, and most of them are intensely stained, with indication of sublamination within this layer (Va and Vb). Layer VI can be subdivided into a superficial layer of intensely stained medium-sized and large neurons (VIa) and a deep layer of smaller, fusiform-shaped cells (VIb; Fig. 5A).

Parvalbumin. As shown in Figure 6E,F, area 36c is characterized by a moderate concentration of parvalbumin-immunoreactive fibers and terminals in the middle layers (mainly layer IV), with very few fibers in the superficial and deep layers. The band of parvalbumin-positive fibers continues laterally into the middle layers of area TEav. In TEav, however, the staining is much denser and extends into layers III and V/VI (Fig. 6G). There are also a relatively large number of parvalbumin-immunoreactive neurons in TEav (Fig. 7C). In contrast, area 36c is characterized by moderate numbers of parvalbumin-immunoreactive neurons in layer IV, with very few neurons in layers III, V, and VI (Fig. 7B).

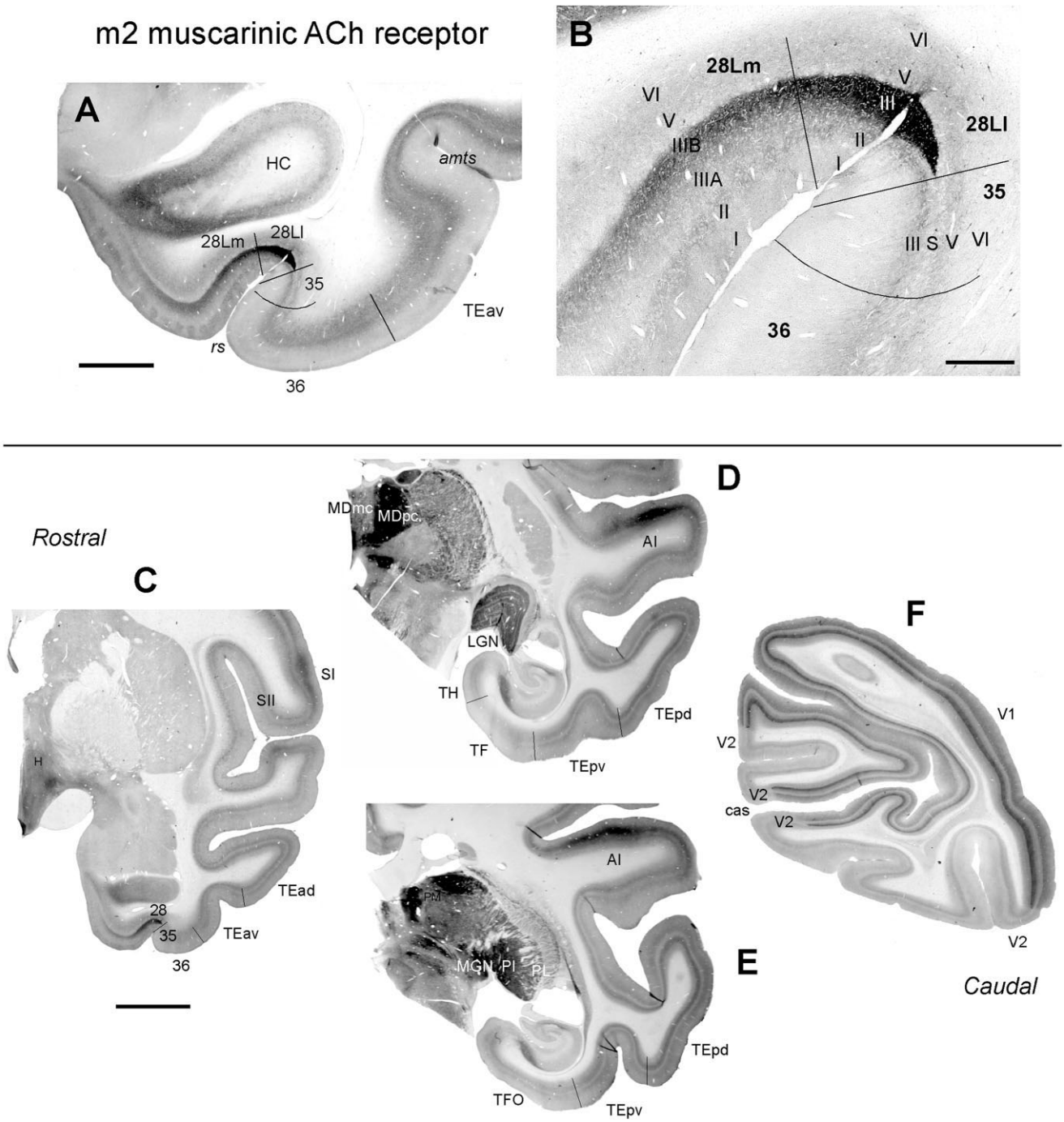

Fig. 4. **A,B:** *M. fuscata*: low- and high-power photographs showing the m2-AChR immunostaining in areas 35, 36, 28, and TE. Note the strongest labeling in the lateral part of the area 28 (28Ll) at the fundus of the rhinal sulcus. **C–F:** *M. fascicularis*: m2-AChR immunostaining in area 28 and other cortical and subcortical areas that showed strong labeling, including the primary somatosensory (SI), auditory (AI), and visual (V1) cortices, and several diencephalic structures (mediodorsal thalamic nucleus, pulvinar, lateral geniculate nucleus, and hypothalamus). Note that there is a moderate double-banded pattern of m2-AChR staining in all subdivisions of area TE, which is sharply reduced in areas TF and TFO (D,E). Scale bars = 2 mm in A; 0.5 mm in B; 5 mm in C (applies to C–F).

SMI-32. In sections stained with the SMI-32 antibody, area 36c is characterized by moderate staining of pyramidal cells and their processes in layers V and VI but relative lack of such staining in layers II and III (Fig. 6I,J). This is particularly distinctive because the medially adjacent area 35 and laterally adjacent area TEav have prominent immunoreactive pyramidal neurons and dendrites in layer IIIb as well as more prominent cell labeling in layer V (Fig. 6K).

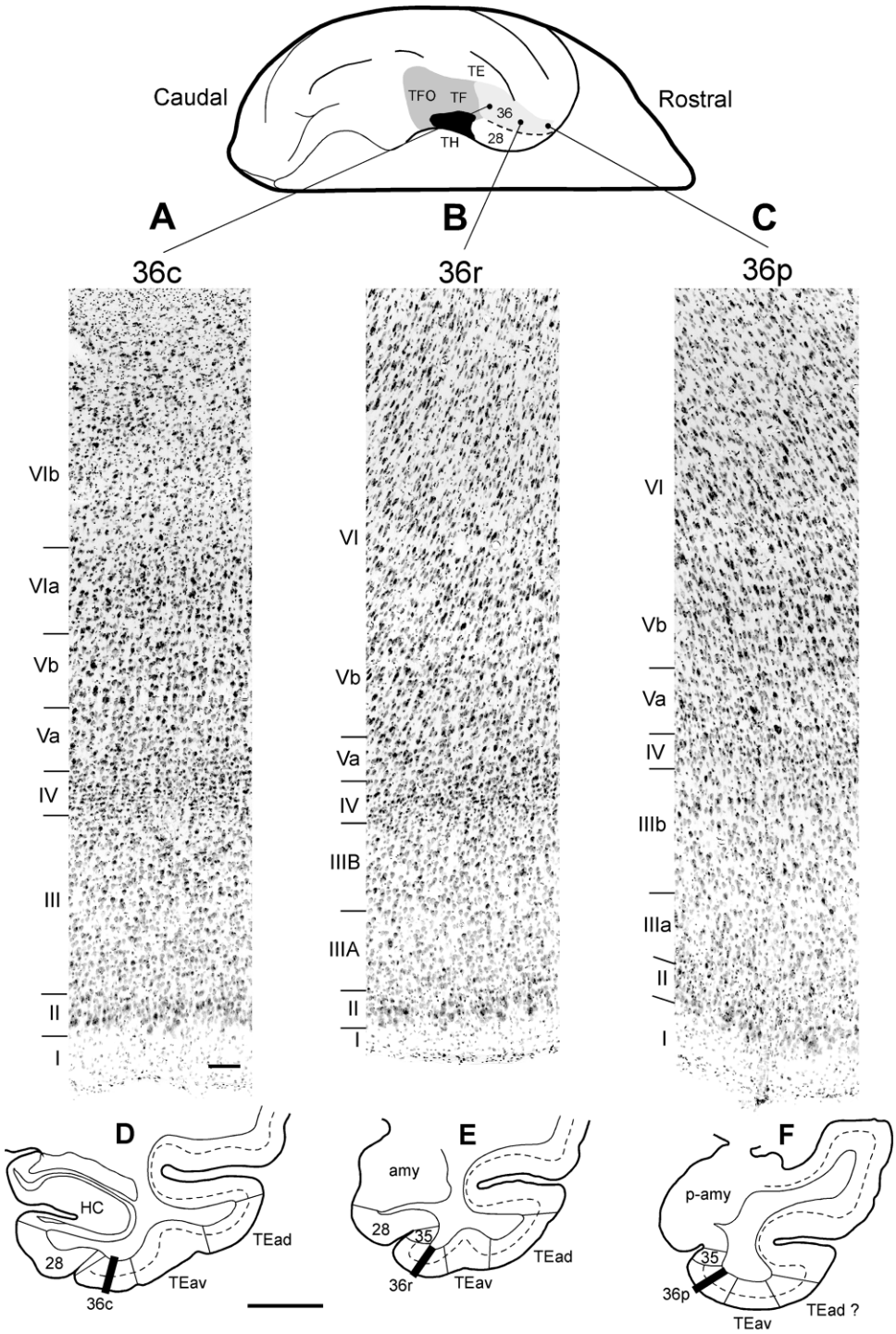

Fig. 5. Three photomicrographs of Nissl-stained sections (**A–C**) illustrate the lamination in the caudal, rostral, and temporal-polar subregions of area 36 (36c, 36r, and 36p, respectively). The approximate location of each photomicrograph is shown on the ventral view of the brain on the top, and the line drawings of coronal sections at the bottom (black rectangles; **D–F**). Note that layer IV is less prominent in 36p than in 36r and 36c. In all of the subregions, layer II is characterized by densely packed patches of cells and layer V by prominent darkly stained pyramidal cells. Scale bars = 100 μm in A (applies to A–C); 5 mm in D (applies to D–F).

Area 36r (rostral subregion of area 36)

Most of the cytoarchitectonic features observed in area 36r are similar to those in area 36c. Layer II of area 36r is more prominent than that in area 36c, and the clusters of neurons are more obvious. Layer III can be subdivided into layer IIIa, with small to medium-sized pyramidal

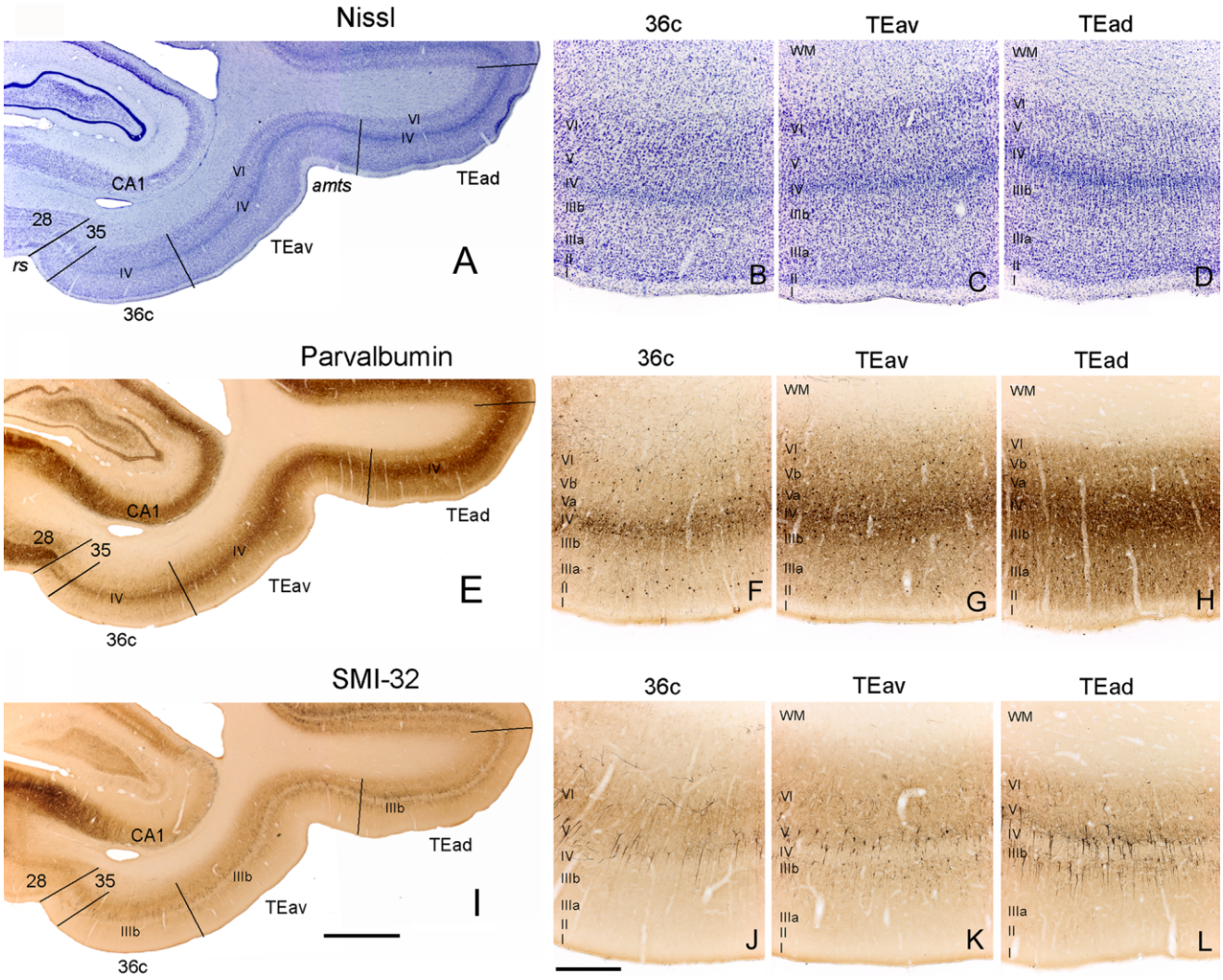

Fig. 6. **A,E,I:** Low-power photomicrographs of Nissl-, parvalbumin-, and SMI-32-stained sections illustrate the mediolateral extent and the architectonic organization of areas 36c, TEav, and TEad. **B–D,F–H,J–L:** Corresponding high-power photomicrographs through the midpoint of these architectonic areas. In Nissl-stained sections, layers IV, V, and VI are clearly distinguished from each other in area TEav and TEad, but less so in area 36c (A–D). There is also a clear decrease in the density of parvalbumin staining and SMI-32 staining of neuronal somata and dendrites in area 36c (F,J). Note that the border between areas 36c and TEav is located approximately halfway between the amts and the rhinal sulcus, and that there is close agreement in the location of this border with all three stains. Scale bars = 2 mm in I (applies to A,E,I); 0.5 mm in J (applies to B–D,F–H,J–L). [Color figure can be viewed in the online issue, which is available at www.interscience.wiley.com.]

cells, and IIIb, with larger pyramidal cells, whereas layer IV is thinner and less distinct than area 36c (Fig. 5B). Layers V and VI contain intensely stained pyramidal neurons similarly to area 36c, with no clear boundary between these layers. The pattern of staining with parvalbumin and SMI-32 in area 36r is also similar to that in area 36c.

Area 36p (temporal-polar subregion of area 36)

Compared with areas 36c and 36r, area 36p has a thinner and less distinct layer IV, and the clusters of cells in layer II are less prominent (Fig. 5C). As in area 36r, layer III of area 36p is subdivided into IIIa, with smaller pyramidal neurons, and IIIb, with many large cells. Layers V and VI also contain intensely stained pyramidal neurons, but they appeared to be more fusiform than in other subregions of area 36. The pattern of parvalbumin and SMI-32 staining is similar to that in the other parts of area 36, although the density of parvalbumin staining is slightly greater in area 36p.

Distinction between area 36p and the temporal pole

Some previous descriptions of the perirhinal cortex have included the cortex on the dorsomedial aspect of the temporal pole as area 36d (Suzuki and Amaral, 1994a, Suzuki and Amaral, 2003; Lavenex et al., 2002) or 36pm and 36pl (Insausti et al., 1987; Munoz and Insausti, 2005; Mohedano-Moriano et al., 2005). Because there are substantial architectonic and connectional differences be-

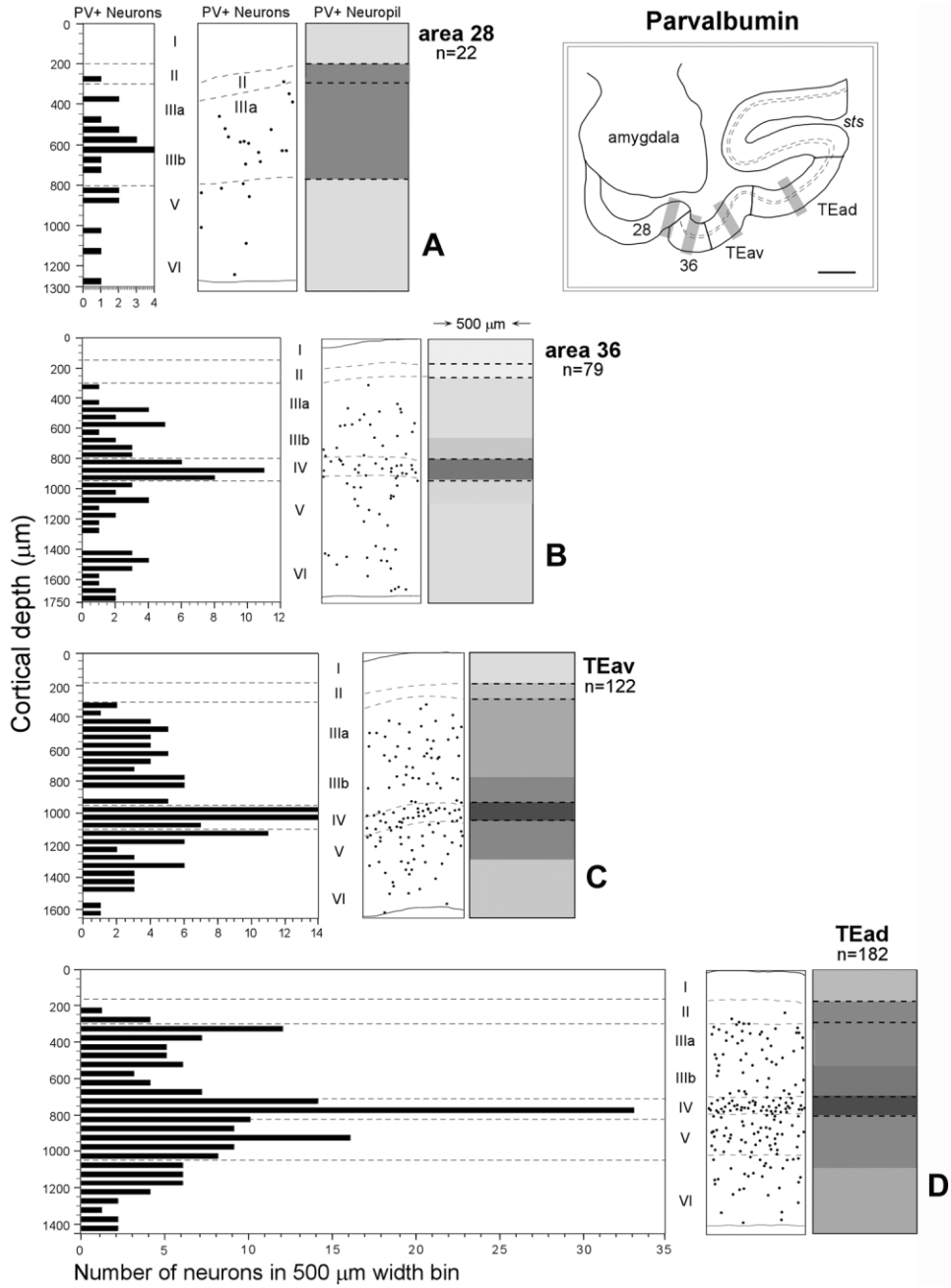

Fig. 7. The spatial and laminar distribution patterns of parvalbumin-stained neurons in entorhinal cortex (area 28), perirhinal cortex (area 36), and areas TEav and TEad (**A–D**). For each area, the histogram at left represents the number of parvalbumin-stained cells in 50-μm bins of a 500-μm traverse through the cortex, at the points marked by the gray stripes in the diagram. The boxes to the right of each graph show the distribution of parvalbumin-positive cells (each dot = one cell). The next boxes on the right provide schematic illustrations of the laminar density of stained fiber and terminal plexus in the neuropil. The number below the area designation (e.g., n = 22) indicates the total number of parvalbumin-immunoreactive cells counted in the traverse. Note that there is a clear increase in the density of immunostained plexus and neurons from area 36 to area TEad, predominantly in the middle layers of these areas (B–D). In area 28, a strongly immunostained plexus was observed in layers II and III (A). Scale bar = 2 mm in diagram.

tween this region and area 36, however, we have not included the dorsomedial temporal pole within area 36 (see Kondo et al., 2003, Kondo et al., 2005). Two areas can be recognized in this region. The first is a dysgranular area that we have previously termed the "dorsal dysgranular" part of the temporal pole (TGdd; Kondo et al., 2003). Embedded within the caudal edge of TGdd, near the limen insula, is a small region that is very rich in parvalbumin immunoreactivity. This area is directly continuous with the parvalbumin-rich auditory core and belt

areas, and it appears to represent the rostral end of this cortical strip, corresponding either to the "rostrotemporal area" (RT; Hackett et al., 1998) or to a small area just rostral to RT. We have termed this area "RTp" ("p," for polar) in this study (see Fig. 9A,D).

The architectonic structures of areas TGdd and RTp differ markedly from those of areas 36p, 36r, and 36c, especially in sections stained for SMI-32 and parvalbumin. Most distinctively, areas TGdd and RTp have a single prominent band of SMI-32-stained cells and processes in layer V (Fig. 8D–F), whereas area 36p contains a double band of staining, in superficial layer V (Va) and in superficial layer VI (VIa; Fig. 8G). In sections stained for parvalbumin, there is a very dense plexus of stained fibers and terminals in layers I and IV of area RTp (Fig. 9D,E). This contrasts with a moderate plexus of fibers and terminals in layer IV in areas 36p (Fig. 9G), 36r, and 36c. Area TGdd, adjacent to area RTp, also has a more moderate and diffuse parvalbumin-positive plexus (Fig. 9D–F).

Although area TGvd more closely resembles area 36p, and has similar connections (Kondo et al., 2003, Kondo et al., 2005), the lamination in area TGvd is less distinct. With SMI-32, the clear distinction between layers Va, Vb, and VIa in area 36p is lost in area TGvd (Fig. 8G–I). Similarly, with parvalbumin immunohistochemistry, the relatively well defined band of staining in layer IV in area 36p becomes less dense and much less distinct in area TGvd (Fig. 9G–I).

Distinction and border between areas 36 and TEav

In Nissl-stained sections, the distinction between areas 36 and TEav is best seen in layers IV, V, and VI, which are clearly distinguished from each other in area TEav but less so in area 36 (Fig. 6A–C). In area TEav, layer V is less densely packed, whereas layers IV and VI are more dense, so the deeper layers have a marked triple banding pattern (dark-light-dark; Fig. 6C). There is also a clear decrease in the density of the parvalbumin-positive plexus in the middle cortical layers from area TEav to area 36 (Fig. 6E–G). With SMI-32 immunostaining, cell labeling is particularly marked in layer V of area TEav, with additional staining in the deeper part of layer III (IIIb) and layer VI. In area 36, labeled neurons are less prominently stained and are confined mainly to layers V and VI (Fig. 6I–K). With all three stains, there is close agreement in the location of the border (Fig. 6, see low-power photomicrographs).

Based on these criteria, the location of the border between areas 36 and TEav varied in relation to the rhinal sulcus and anterior middle temporal sulcus (amts) at different rostrocaudal levels. Caudally, the border is located approximately midway between the amts and the rhinal sulcus (Figs. 1C, 6). More rostrally, the border is shifted laterally to a point near the medial lip of the amts (Fig. 1B,G).

Rostral to the amts, the distinction between areas TEav and 36p is slightly different. In this part of area TEav, layers V and VI are less distinct. The main architectonic features that distinguished area 36p from area TEav are the darkly stained fusiform pyramidal neurons in layer V of area 36p, and the more prominent granular layer IV and associated parvalbumin-positive plexus in area TEav (Fig. 1A).

Distinction and border between areas TEav and TEad

Although this paper is focused on the perirhinal and parahippocampal areas, and areas immediately adjacent to them (entorhinal and TEav), it is useful to consider the distinction between areas TEad and TEav in order to compare our results with previous descriptions that extended area 36 more laterally, into what we consider area TEav (Suzuki and Amaral, 1994a, Suzuki and Amaral, 2003). The architectonic structure of these areas was previously described briefly in relation to their connections (Saleem and Tanaka, 1996; Saleem et al., 2000), but these descriptions did not include full details of staining with SMI-32 or parvalbumin.

The main difference between areas TEad and TEav is the arrangement of cells in the middle layers. Layers IIIb and Va are more prominent in area TEad than in TEav, and the neurons are more aligned in radial columns (Fig. 6D). Layer Vb is less dense in area TEad than in area TEav. In the sections stained immunohistochemically for parvalbumin, there is a clear decrease in the density of neuropil staining at the border from area TEad to area TEav (Fig. 6E–H). The intense staining of neuropil in area TEad is also coupled with relatively large numbers of parvalbumin-immunoreactive neurons (Fig. 7D). These features are observed throughout the rostrocaudal extent of areas TEad and TEav. Layer I of area TEad also contains many prominent vertically oriented dendrites of chandelier neurons, although these are more sparse in area TEav. In sections stained for SMI-32, there is a dense labeling of pyramidal neurons in layers IIIb and layer V of area TEad, which becomes more moderate in area TEav (Fig. 6K,L). The border between areas TEav and TEad determined by these criteria was located at the lateral bank or lip of the amts caudally but is near the sts farther anteriorly.

Areas 35 and 36 in *M. fascicularis*, *M. fuscata*, and *M. mulatta*

We also compared the architectonic organization of areas 35 and 36 in cynomolgous monkeys (*M. fascicularis*) with that in Japanese monkeys (*M. fuscata*) and rhesus monkeys (*M. mulatta*). In general, the location and cytoarchitectonic features of area 35 and its border with area 28 are similar in all three species of macaques (Fig. 10).

As shown in Figure 11, the border between area TEav and the caudal part of area 36 is located halfway between the amts and the rhinal sulcus in all three species of macaques. As in *M. fascicularis*, the border in *M. fuscata* and *M. mulatta* is based primarily on the architectonic distinction that layers IV, V, and VI are clearly distinct in area TEav, whereas they are relatively fused together in area 36 (Fig. 11).

Cytoarchitectonic and chemoarchitectonic subdivisions of the parahippocampal cortex (areas TH and TF/TFO)

The parahippocampal cortex is located in the posterior parahippocampal gyrus (Van Hoesen, 1982) and consists of two distinct cytoarchitectonic regions, areas TH and TF (von Bonin and Bailey, 1947). Rostrocaudally, the architectonic characteristics of parahippocampal cortex, especially area TF, are more heterogeneous than those of the perirhinal cortex (see below).

Area TH

Area TH is a relatively small, agranular cortical region that extends about 4–5 mm caudal to the entorhi-

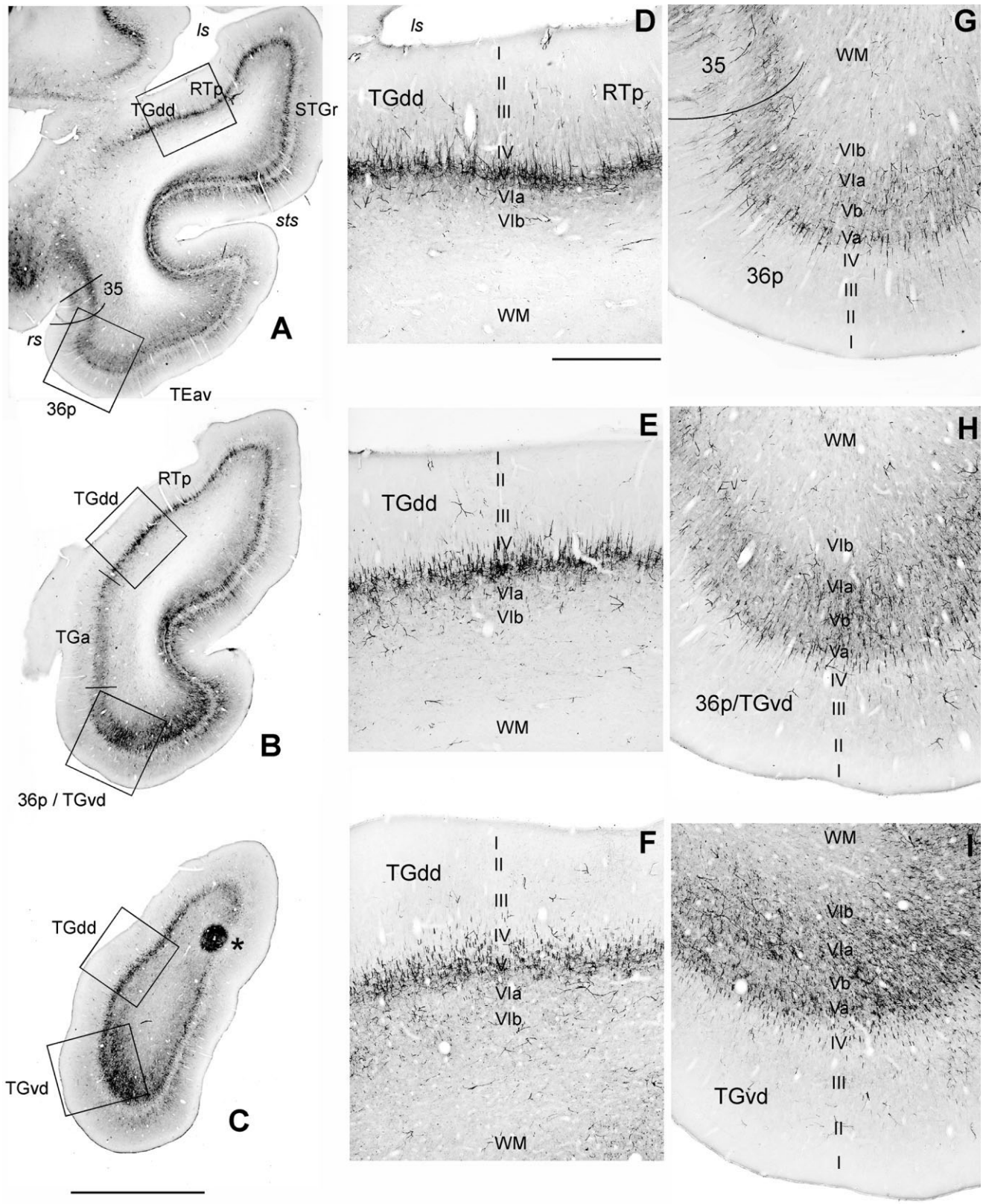

Fig. 8. Chemoarchitectonic comparison between the dorsomedial (RTp and TGdd) and ventromedial (TGvd) temporal pole and the perirhinal cortex (36p) in sections stained with SMI-32. Low-power photomicrographs are arranged from caudal to rostral (**A–C**). The boxed areas in the dorsomedial temporal pole regions are shown in high-power photomicrographs in **D–F**, and the perirhinal cortex and ventromedial temporal pole region are illustrated in **G–I**. A dark spot in C (asterisk) shows the tracer injection site in the dorsolateral temporal pole (see also Fig. 9C), which was used in different studies. Note that both area RTp and area TGdd have a single prominent band of SMI-32-labeled pyramidal cells and processes mainly in layer V (D–F). In contrast, areas 36p and TGvd have a double band of pyramidal cells in layers Va and VIa, although the distinction between these layers is less clear in TGvd (G–I). Scale bars = 5 mm in C (applies to A–C); 1 mm in D (applies to D–I).

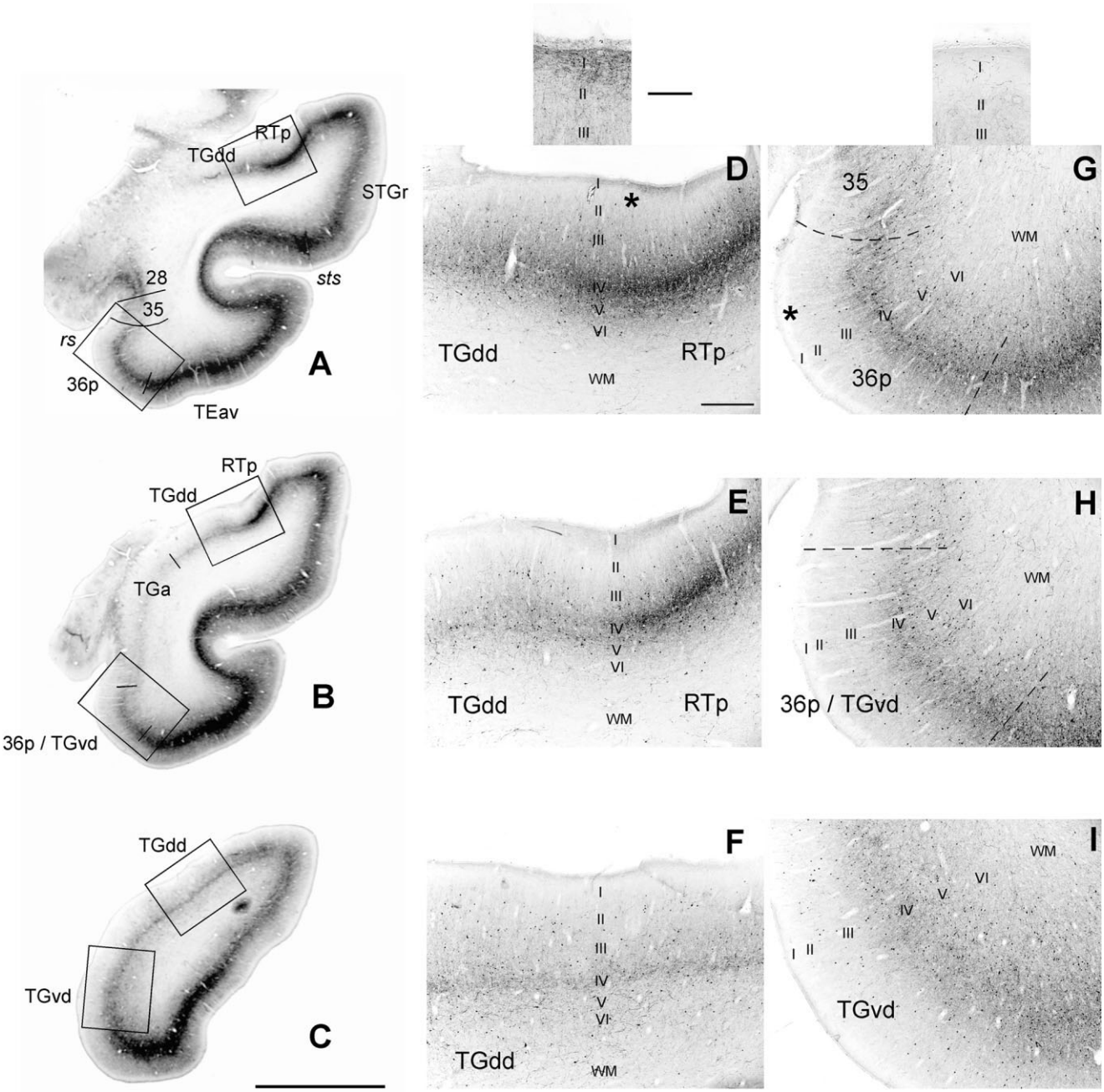

Fig. 9. Chemoarchitectonic comparison between the dorsomedial (RTp and TGdd) and ventromedial (TGvd) temporal pole and the perirhinal cortex (36p) in parvalbumin-stained sections. Three low-power photomicrographs are arranged from caudal to rostral (**A–C**). The boxed areas in the dorsomedial temporal pole regions are shown in high-power photomicrographs in **D–F**, and the perirhinal cortex and ventromedial temporal pole region are illustrated in **G–I**. The two high-power photomicrographs on the top are taken from areas RTp and 36p in D and G (asterisks). Note that RTp has a dense plexus of fiber staining in layer IV and layer I, which is absent in 36p (D,G). Scale bars = 5 mm in c (applies to A–C); 0.5 mm in D (applies to D–I); 100 μm in photomicrographs at the top.

nal cortex and medial to area TF (Fig. 1G). Area TH is relatively homogeneous, and we did not recognize rostrocaudal subdivisions within it (cf. Suzuki and Amaral, 2003; Blatt et al., 2003). At the rostral edge of area TH, near the entorhinal cortex, however, there are clusters of neurons in layer II that are not seen farther caudally. These are markedly different from the cell islands in layer II of the entorhinal cortex (Fig. 12A–C).

Nissl. Area TH is characterized by the lack of layer IV and a prominent, darkly staining layer V (Fig. 12B,C). Rostrally, layer II is marked by rounded clusters of neurons, which extend into layer III; these are considerably thicker than the thin cell islands of layer II in the entorhinal cortex (Fig. 12A,B,E,F). More caudally, the neuronal clusters disappear, and layer II blends into a thick, homogeneous layer III (Fig. 12C,G). Layer V is composed

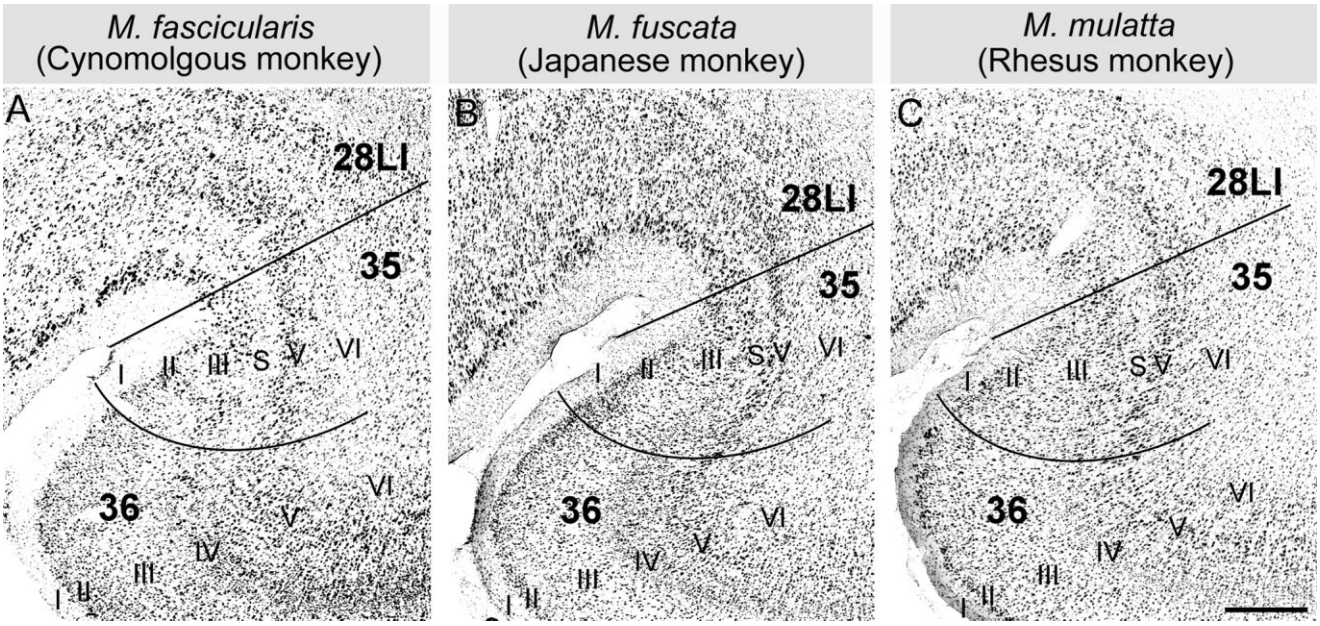

Fig. 10. Sections through areas 28, 35, and 36 in three macaque species, stained with the Nissl method (**A–C**). Note that the cytoarchitectonic organization of area 35 is similar in all of the species. Labels and conventions are the same as in Figures 2 and 3. Scale bar = 0.5 mm.

of large, darkly staining pyramidal cells and has relatively sharp superficial and deep borders (Fig. 12B,C,J,K). These features are clearly distinct from those of layer V of the entorhinal cortex (Fig. 12A–C). Layer VI is very distinct in the rostral part of area TH but becomes lighter and less clearly demarcated from the white matter caudally. Caudally, area TH is replaced by area TFO (see below), which has a distinct granular layer IV (Fig. 12D). In area TFO, the densities of layers V and VI are reversed, such that layer V is light and layer VI dark (compare Fig. 12C and D).

Parvalbumin. Area TH stains relatively lightly for parvalbumin. This provides a marked distinction from the entorhinal cortex, where layers II and III are very darkly stained, and from area TFO, where there is dark staining in the middle layers of the cortex (Fig. 13A–D). Within area TH, there is a slight rostrocaudal gradient from very light staining rostrally to more moderate staining caudally (Fig. 13B,C).

SMI-32. At the rostral edge of area TH, there is only very light staining of neurons in layer V with SMI-32. The staining in layer V increases slightly in the caudal part of area TH but does not extend into other layers (Fig. 13F,G). This provides a clear distinction between area TH and the entorhinal cortex, where there is strong staining in layer II, and between areas TH and TFO, where there is good staining of cells in layer IIIb as well as layers V and VI (Fig. 13E–H).

Areas TF and TFO

We found consistent rostrocaudal differences in the architectonic characteristics of area TF, especially in layers IV, V, and VI (Fig. 14). Based on these variations, and on differences in connections between rostral and caudal parts, we separated the caudal region from area TF and termed it "area TFO," following a similar designation by Blatt et al. (Blatt et al. 2003; see discussion; Fig. 1). However, our area TFO corresponds to areas THO and TLO of Blatt et al. (2003) but does not include more lateral area that they labeled TFO. We did not recognize mediolateral subdivisions within area TF or TFO (cf. Suzuki and Amaral, 2003).

Areas TF and TFO extend roughly 3–7 mm in the mediolateral direction from area TH to area TEpv and, taken together, extend 8–9 mm in the rostrocaudal direction from the perirhinal cortex to area V4, which is marked by the beginning of the calcarine sulcus. Whereas area TF is dysgranular, area TFO has a prominent layer IV and can be considered granular cortex (Fig. 14A,B). The architectonic features of area TFO closely resemble those of the caudally adjacent visual area V4, although some architectonic differences between them are evident (see below). The architectonic borders between areas TF and TFO and between areas TFO and V4 are less sharp than the borders between areas TF and TEpv.

Nissl. In the Nissl-stained sections, area TF is characterized by a relatively homogeneous density of layers IV, V, and VIa, which are relatively darkly stained, and of layers II and III, which are relatively lightly stained (Fig. 14A). It is distinguished from the rostrally adjacent area 36c primarily by the patches of large, darkly stained, round cells in layer II of 36c and the more uniform layer II in area TF (compare Figs. 5A and 14A). The other layers are similar to those in area 36, although layer III is more uniform. As mentioned above, area TFO is more granular than area TF (Fig. 14B). Layer VI of TFO is also more dense, such that layer V can be distinguished as a lighter band between the darker layers IV and VI.

Parvalbumin. Area TF is characterized by a sparse parvalbumin-immunoreactive plexus in layer IV, with little staining in other layers (Fig. 15A). This is particularly

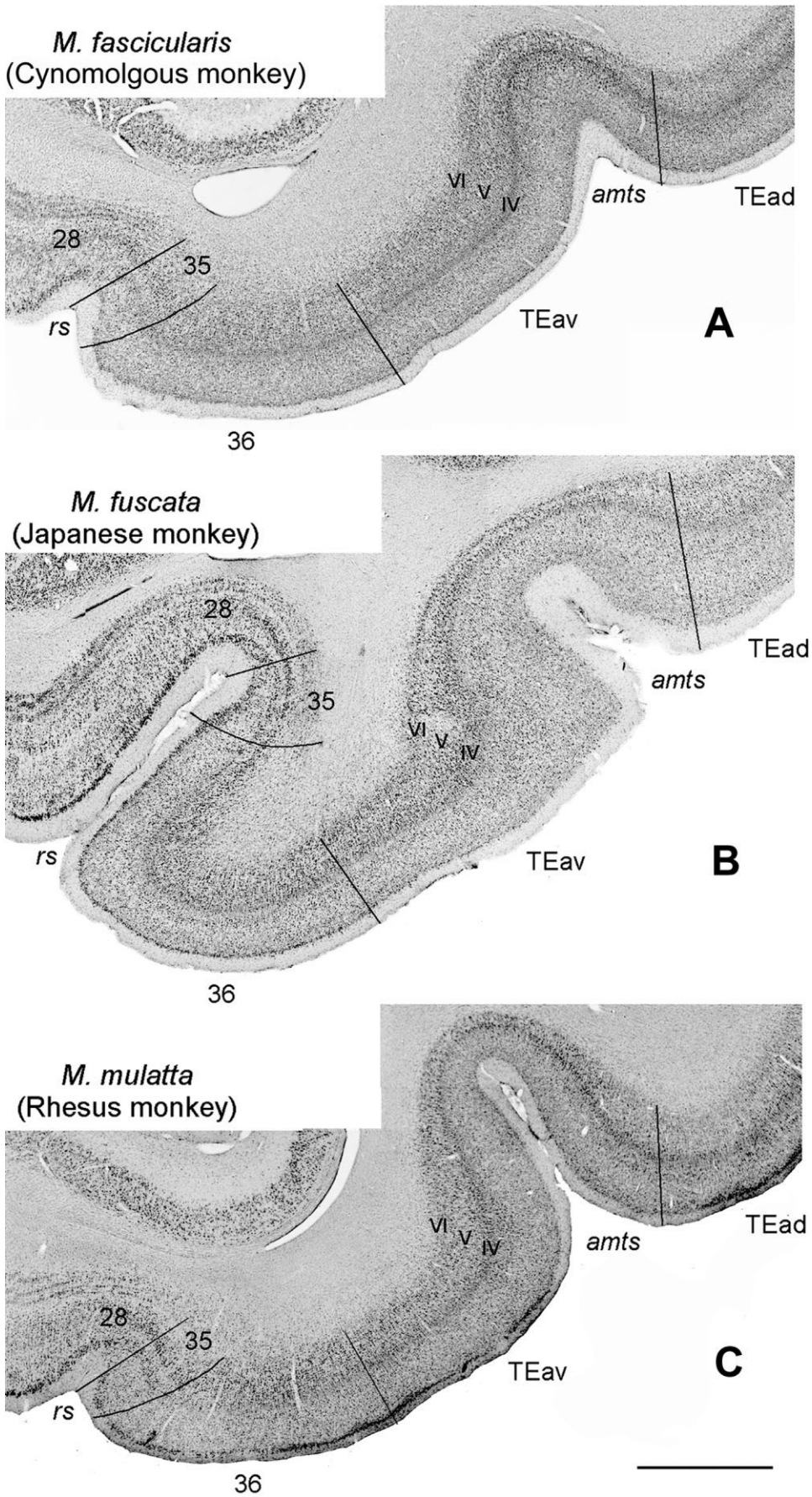

Fig. 11. Cytoarchitectonic organization and borders of areas 35 and 36 in three macaque species (**A–C**). Note that, in all three species of macaques, the border between areas 36 and TEav is located approximately midway between the amts and the rhinal sulcus. Scale bar = 2 mm.

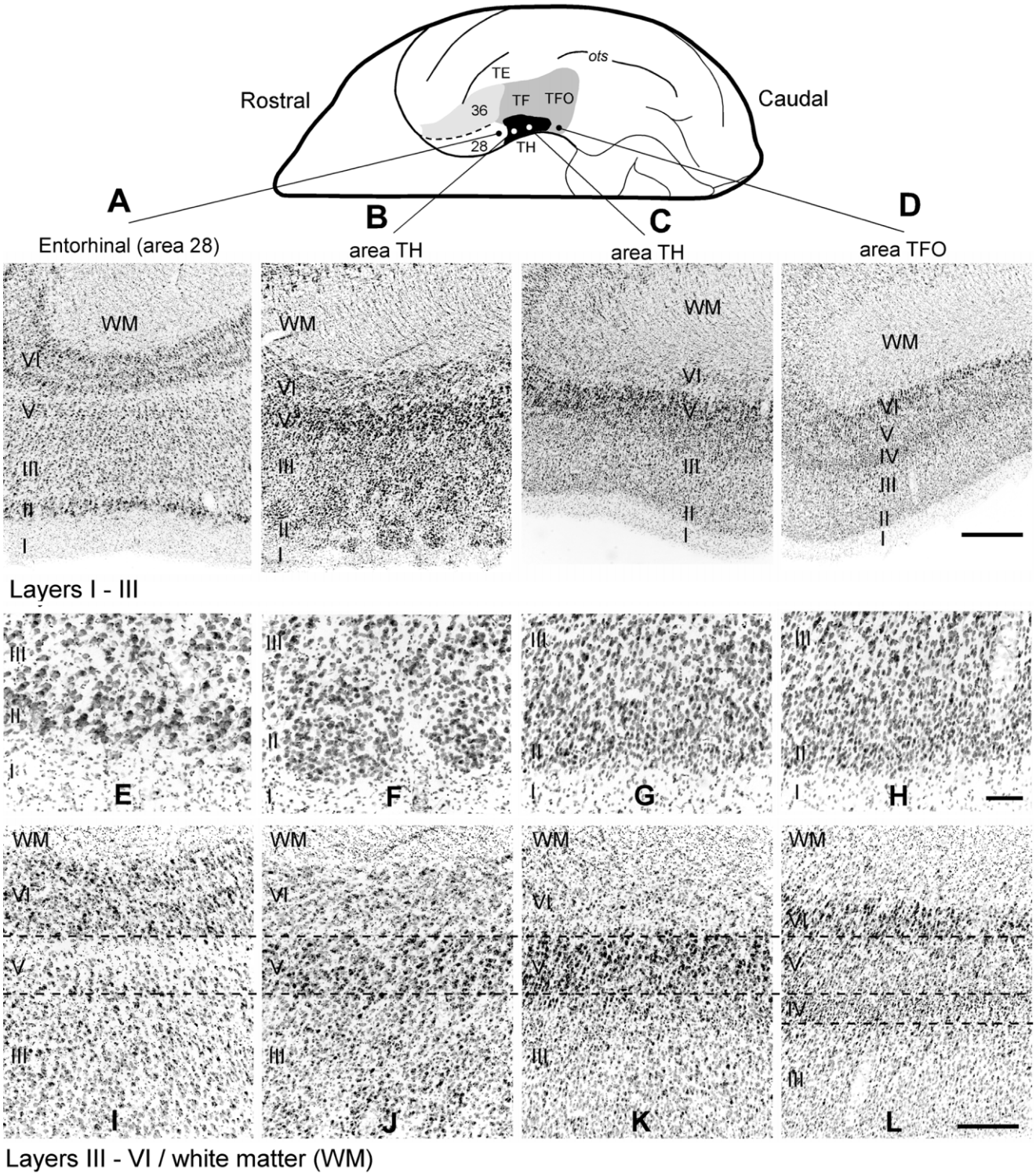

Fig. 12. Laminar organization of area TH and the adjacent areas. **A–D:** Four low-power photomicrographs arranged from rostral to caudal showing the lamination in areas 28, TH, and TFO. The approximate locations of these photomicrographs are indicated on the ventral surface of the brain at top. **E–H:** High-power photomicrographs from the same areas to illustrate layers I–III. Note that there are clusters of neurons in layer II at the rostral edge of area TH (F) that are not seen further caudally (G). These clusters are markedly different from the cell islands in layer II of area 28 (E). **I–L:** High-power photomicrographs from the same areas showing layers III–VI. Layer IV is absent in area TH but present in TFO (K, L). Layer V in area TH is more distinct than in areas 28 and TFO, with large, darkly stained neurons. Scale bars = 0.5 mm in D (applies to A–D); 100 μm in H (applies to E–H); 200 μm in L (applies to I–L).

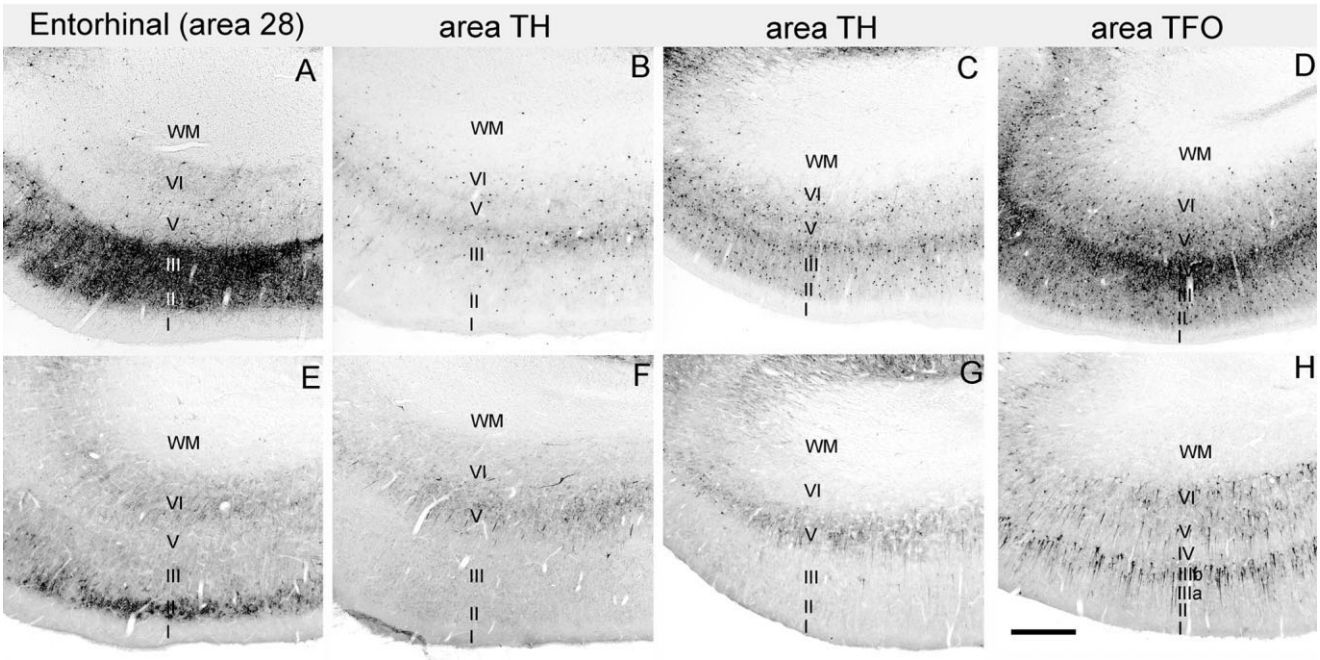

Fig. 13. Photomicrographs, arranged from rostral to caudal, showing the distribution of parvalbumin-stained fiber and terminal plexus and neurons (**A–D**) and SMI-32-stained neurons (**E–H**) in area 28, rostral and caudal area TH, and area TFO (see Fig. 12). Note that there is much greater parvalbumin and SMI-32 staining in area 28 and in area TFO than in area TH. Scale bar = 0.5 mm.

distinctive in relation to the much greater density of parvalbumin-immunoreactive neuropil and neurons in layers II–VI (concentrated in layer IV) of areas TEpv, TFO, and V4 (Figs. 1D–F, 15B,C).

SMI-32. Area TF is distinguished by a band of SMI-32-labeled pyramidal neurons in layers V and VI, with very few or no labeled neurons in layers II and III (Fig. 15D). This is particularly distinctive because the caudally adjacent areas TFO and V4 have prominent SMI-32 positive pyramidal neurons and dendrites in layer IIIB, in addition to the staining in layers V and VI (Fig. 15E,F).

Distinction between area TFO and area V4

Although areas TFO and V4 closely resemble each other in cytoarchitectonic features, V4 is more granular, and the cells are arranged more radially than in area TFO (Fig. 14C). In addition, parvalbumin staining is more intense in area V4 and extends into more superficial layers (Fig. 15C). With SMI-32, the staining in area V4 is much more intense in layers IIIb and V/VI and also extends into layers IIIa and II (Fig. 15F). This pattern of labeling in V4 is essentially the same as that described by Hof and Morrison (1995).

Distinction between and border of areas TF and TFO with area TEpv

The distinction between areas TF and TEpv is comparable to that described above between areas 36 and TEav and is most clearly seen in layers IV–VI (Figs. 6A, 16A). Layers IV and VI are considerably thicker and more prominent in area TEpv, whereas layer V is less densely packed than in area TF. As in TEav, this produces a dark-light-dark pattern in TEpv that is not seen in area TF (Fig. 16A). Sections stained for m2-AChR also show a trilaminar pattern in area TEpv, although the darkly stained bands are in layers IIIb and V, with layer IV being relatively light. This pattern is much less apparent in area TF (Fig. 4D).

The greater prominence of layer IV in area TEpv with the Nissl stain is also reflected by a markedly greater neuropil and neuronal staining for parvalbumin in the middle layer (Figs. 16B, 18C). With SMI-32 immunostaining, cell labeling is particularly marked in layers V and VI of area TEpv, with additional staining in the layer IIIb. In area TF, labeled neurons are less prominently stained and are confined mainly to layers V and VI (Fig. 16F–H). With all three stains, there is close agreement in the location of the border between areas TEpv and TF (Fig. 16). Based on these observations, the lateral boundary of area TF in *Macaca fascicularis* is 2.5–3 mm medial to the medial lip of the ots. This border between areas TF and TEpv also matches the distribution of labeled neurons after retrograde tracer injections into subregions of area TE (see below; Fig. 21).

The architectonic distinction between areas TFO and TEpv is less prominent than that described above between areas TF and TEpv (Fig. 17), although layer IV in area TFO is less prominent and layer VI is more densely packed than in area TEpv. In both areas, there is a dark-light-dark pattern in layers IV–VI (Fig. 17A). Based on the Nissl-stained sections, the border between areas TFO and TEpv is located close to the medial lip of the ots. This is more lateral than the border between areas TF and TEpv.

Staining for parvalbumin in the middle layers of area TFO is very similar to that in area TEpv (Fig. 17B), and the number of parvalbumin-stained neurons is relatively uniform across these areas (Fig. 19A,B). Likewise, staining for SMI-32 in layers IIIb and V/VI is similar in both areas (Fig. 17C). Thus, it is difficult to distinguish area

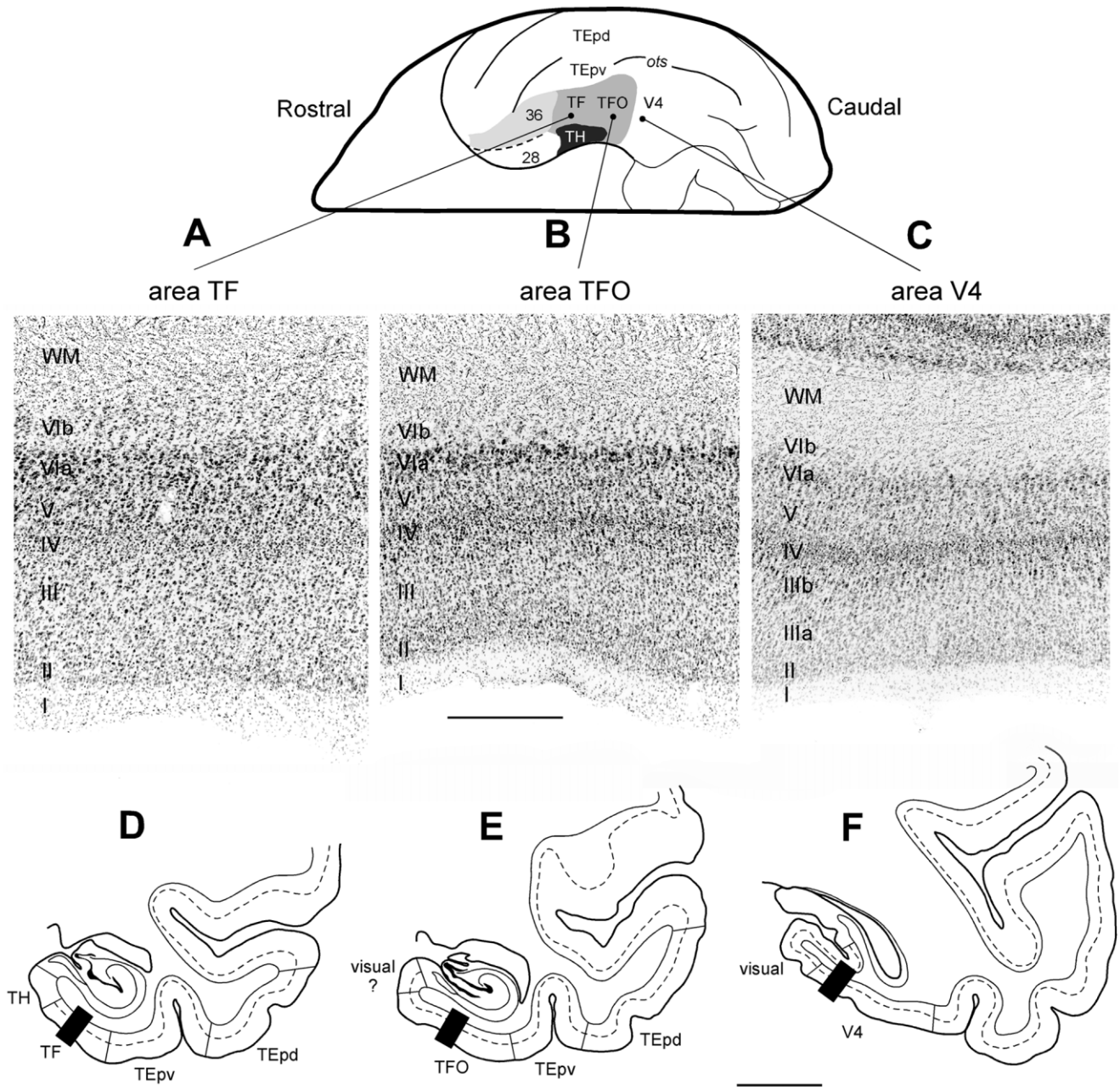

Fig. 14. Photomicrographs arranged from rostral to caudal showing the lamination in areas TF, TFO, and V4 (**A–C**). The approximate locations of these photomicrographs are shown on the ventral view of the brain at top and on coronal sections at bottom (black rectangles; **D–F**). Note that layer IV is progressively more prominent in areas TFO and V4 compared with area TF. Layer V is relatively sparse in areas TFO and V4. Scale bars = 0.5 mm in B (applies to A–C); 5 mm in F (applies to D–F).

TFO from area TEpv in parvalbumin- and SMI-32-stained sections.

Distinction and border between areas TEpv and TEpd

The distinction between areas TEpv and TEpd is similar to that described above between areas TEav and TEad (see Fig. 6). The major difference is in the superficial layers, which contain more parvalbumin and SMI-32 staining in TEpd. With parvalbumin, layer I of TEpd contains many prominent vertically oriented dendrites of chandelier neurons, whereas these are sparse in area TEpv (Fig. 16D,E). Furthermore, SMI-32-labeled pyramidal neurons in layers II, III, and V are more prominent in area TEpd than in area TEpv (Fig. 16H,I). The border between areas TEpv and TEpd determined by these criteria was located at the lateral bank or lip of the ots.

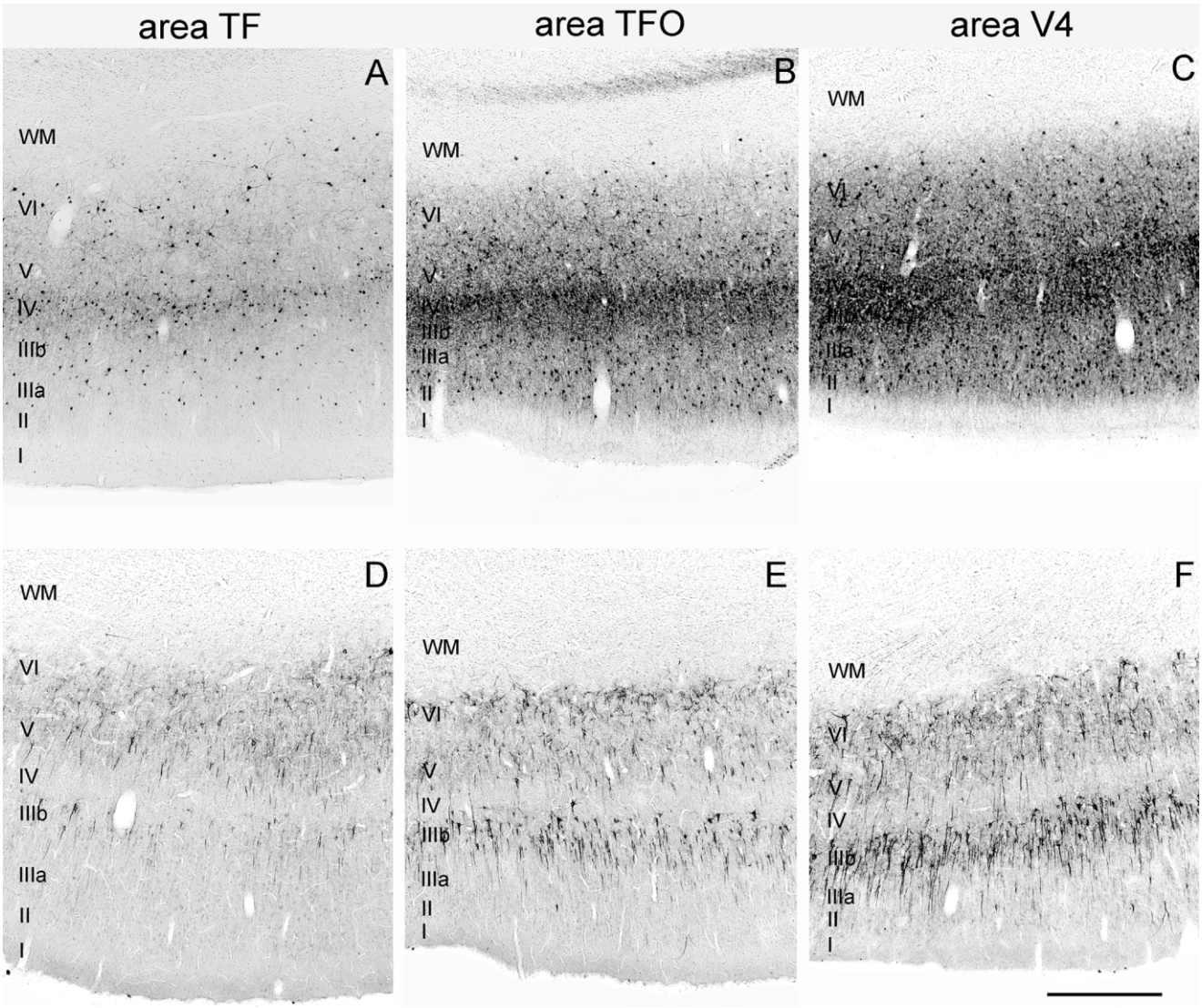

Fig. 15. Photomicrographs, arranged from rostral to caudal, showing the distribution of parvalbumin-stained fiber and terminal plexus and neurons (**A–C**) and SMI-32-stained neurons (**D–F**) in areas TF, TFO, and V4. The approximate locations of these photomicrographs are shown on the ventral view of the brain in Figure 14. Note that there is progressively greater parvalbumin staining in layer IV, and many SMI-32-stained neurons in layer IIIb, going from area TF to areas TFO and V4. Scale bar = 0.5 mm.

Areas TF and TH in *M. fascicularis*, *M. fuscata*, and *M. mulatta*

The architectonic structure of areas TF and TH is similar in *M. fascicularis*, *M. mulatta*, and *M. fuscata*. The relation of the lateral boundary of TF with area TEpv to the ots, however, differs in *M. fuscata* from that in the other species. In *M. fuscata*, this boundary is in the medial bank of the ots, but it is about 3 mm medial to the ots in *M. fascicularis* and *M. mulatta* (Fig. 20A–C). This is very prominent in Nissl-stained material, where the loss of the trilaminate dark-light-dark pattern in layers IV, V, and VI clearly marks the transition from areas TEpv to TF.

Connections of areas TEad and TEav with the parahippocampal cortex

In addition, connections of areas TF and TH that are labeled by tracer injections in other temporal or frontal cortical areas show the same boundaries and the same difference between *M. fascicularis* and *M. fuscata*. Although these connections are not the major focus of this paper, they will be presented as additional evidence for the architectonic delineations.

Injections of WGA-HRP were made in areas TEad and TEav in both *M. fascicularis* and *M. fuscata* (Figs. 21, 22). After the area TEad injections, retrogradely labeled neurons were distributed mainly in layers V and VI of both areas TF and TH (Fig. 21A,B). In addition, anterogradely labeled ax-

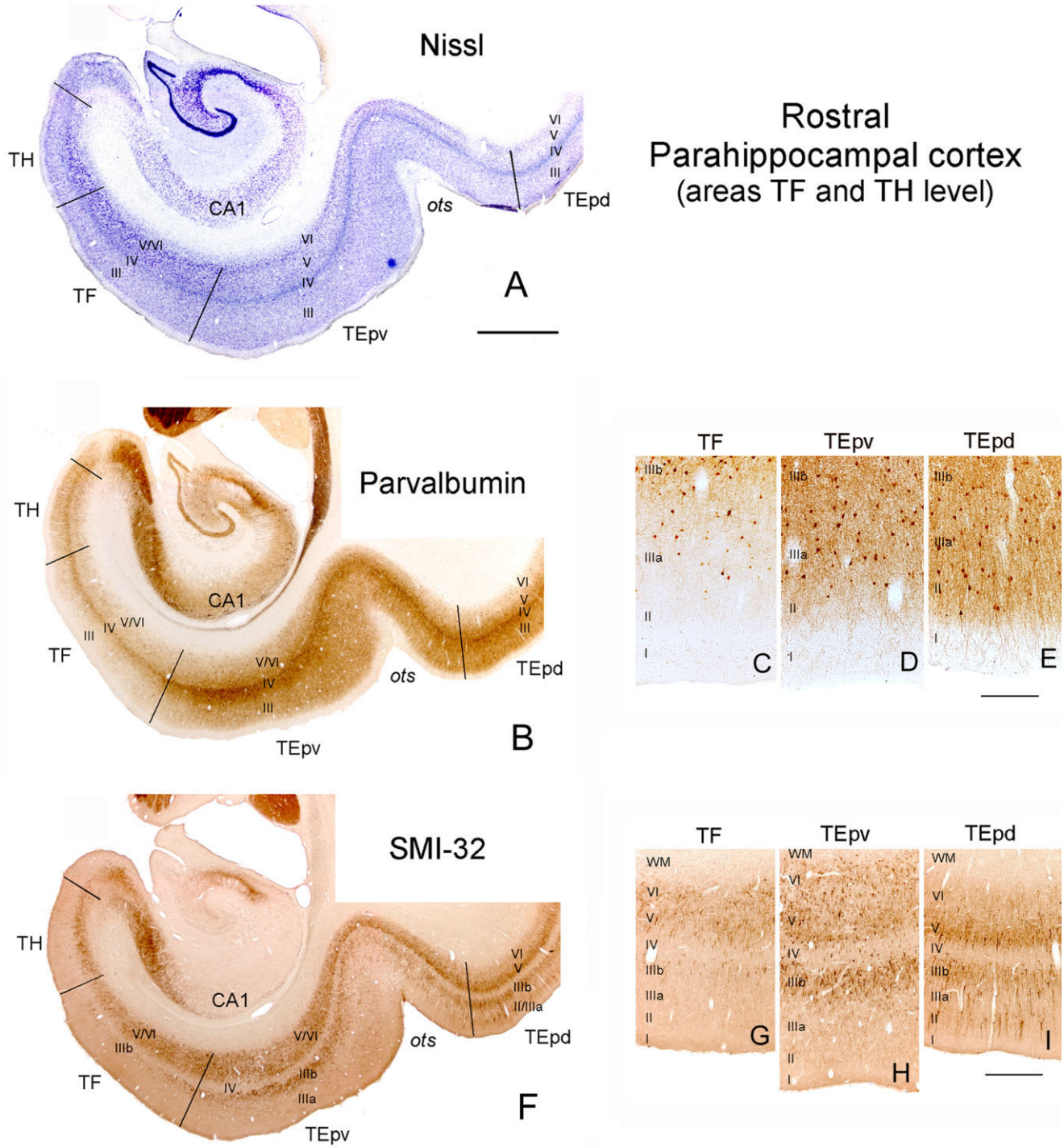

Fig. 16. **A,B,F:** Low-power photomicrographs of Nissl-, parvalbumin-, and SMI-32-stained sections, respectively, illustrate the mediolateral extent and the architectonic organization of areas TF, TEpv, and TEpd. Corresponding high-power photomicrographs from the parvalbumin (**C–E**)- and SMI-32 (**G–I**)-stained sections, spanning different cortical layers through the midpoint of the architectonic areas are also shown. In the Nissl-stained section, layers IV, V and VI are clearly distinguished from each other in areas TEpd and TEpv, but less so in area TF (A). The border between TF and TEpv is also marked by a decrease in the density of parvalbumin staining (B) and by lack of staining in layer III with SMI-32 (F). Note that, with all three stains, the border between areas TF and TEpv is located 2–3 mm medial to the lip of the ots. Scale bars = 2 mm in A (applies to A,B,F); 0.2 mm in E (applies to C–E); 0.5 mm in I (applies to G–I). [Color figure can be viewed in the online issue, which is available at www.interscience.wiley.com.]

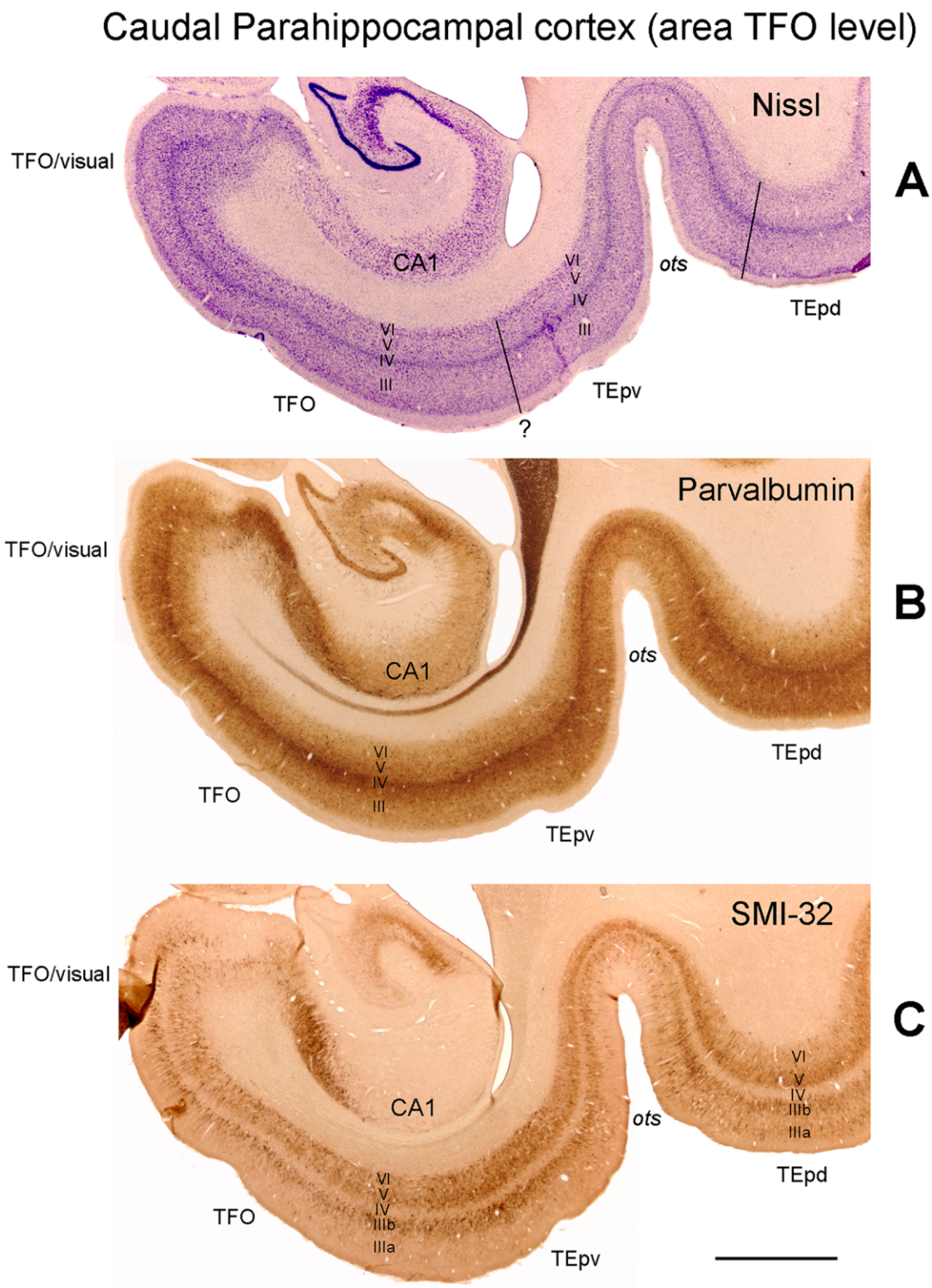

Fig. 17. **A–C:** Low-power photomicrographs of Nissl-, parvalbumin-, and SMI-32-stained sections, respectively, illustrate the architectonic organization of areas TFO, TEpv, and TEpd. In contrast to area TF, area TFO resembles area TEpv in all three stains, although the areas can be distinguished at higher magnification in Nissl stained sections. Scale bar = 2 mm. [Color figure can be viewed in the online issue, which is available at www.interscience.wiley.com.]

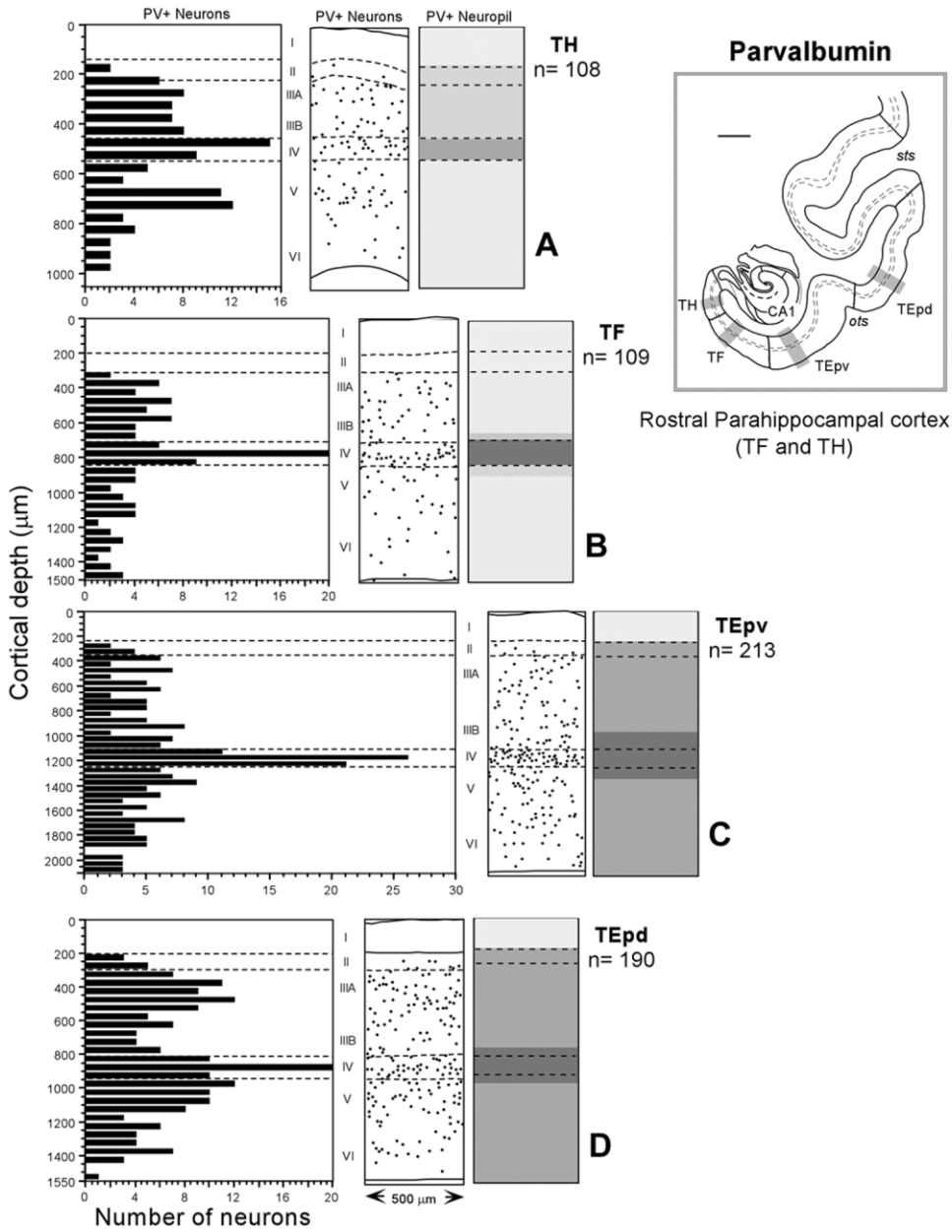

Fig. 18. **A–D:** Spatial and laminar distribution patterns of parvalbumin-stained neurons in the rostral parahippocampal cortex and adjacent areas (areas TH, TF, TEpv, and TEpd. respectively). The graphs and drawings are the same as in Figure 7. Note that there is a clear increase in the density of immunostained fiber and terminal plexus, and neurons from area TF to TEpv, predominantly in the middle layers of these areas (B,C). Scale bar = 2 mm in diagram.

ons were found in more superficial layers of restricted parts areas TF and TH; superficial neuronal label was also found in parts of TF that contained labeled axons. In both species, the labeled neurons and axons were largely restricted to the boundaries of areas TH and TF and with few exceptions did not extend into the entorhinal cortex or into areas TEpv and TFO. In *M. fascicularis*, this meant that the label was limited to the medial part of the parahippocampal gyrus (Fig. 21A). In *M. fuscata*, however, the label occupied the full width of the parahippocampal gyrus and extended into the medial bank of the ots (Fig. 21B). We found a similar distribution of both anterogradely labeled axons and retrogradely labeled neurons in area TF and TH after tracer injections into the orbital and medial prefrontal cortex in *M. fascicularis* monkeys (Kondo et al., 2005).

In both species, the injections in area TEav labeled cells and axons in areas 36 and TEpv, but there were very few labeled cells in area TF or TH (Fig. 22A,B). Labeled cells and axons were distributed in both superficial and deep layers of area TEpv. In *M. fascicularis*, the label occupied the medial bank and lip of the ots (Fig. 22A), but, in *M. fuscata*, the label was almost totally restricted to the lat-

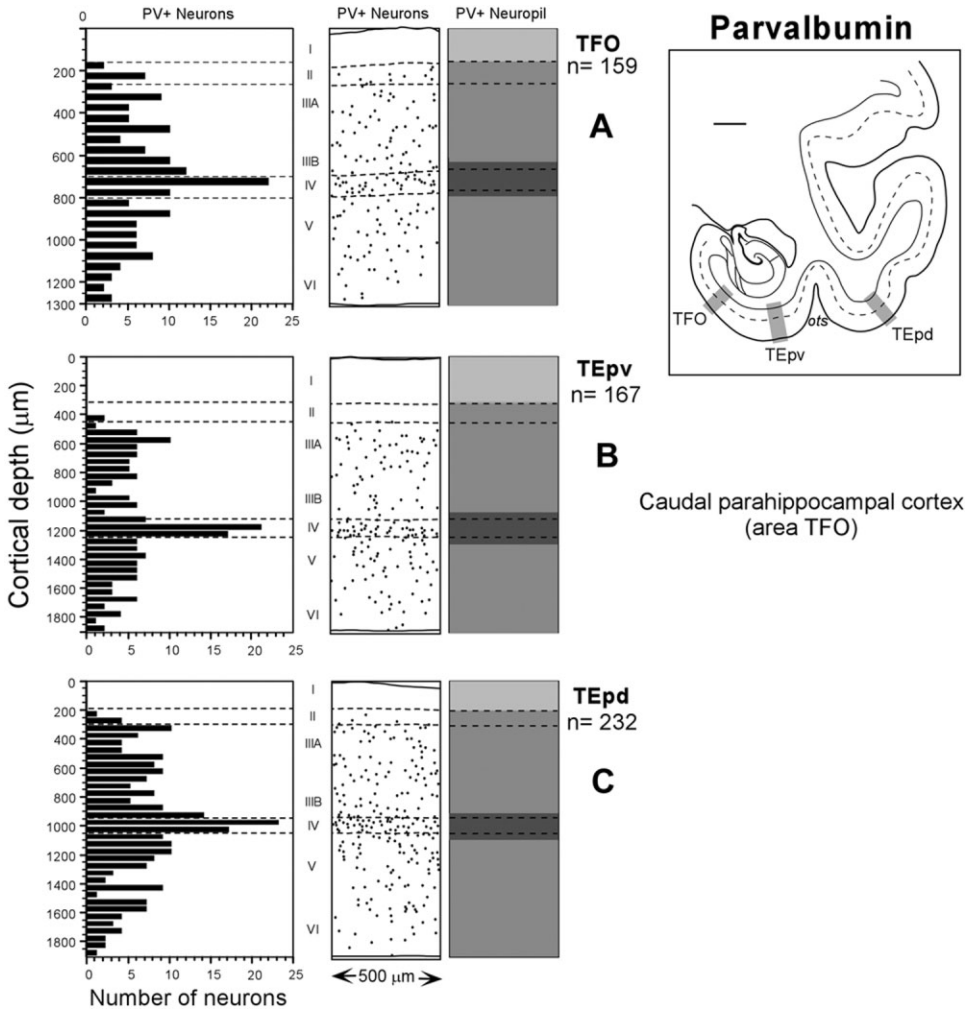

Fig. 19. **A–C:** Spatial and laminar distribution patterns of parvalbumin-stained neurons in the caudal parahippocampal cortex and adjacent areas (areas TFO, TEpv, and TEpd, respectively). The graphs and drawings are the same as in Figures 7 and 18. Note that areas TFO and TEpv are relatively similar to each other (**A,B**), in contrast to the difference between areas TF and TEpv seen in Figure 18. Scale bar = 2 mm in diagram.

eral bank of the ots (Fig. 22B). The distribution of labeled cells and axons agreed with the boundary between areas TEpv and TF that was determined by architectonic criteria.

DISCUSSION

We have described the detailed cytoarchitectonic and chemoarchitectonic characteristics and boundaries of the perirhinal (areas 35 and 36) and parahippocampal (areas TF and TH) cortices in three species of macaque monkeys, with four different staining methods. The key findings are that 1) we did not extend the perirhinal cortex into the temporal pole; 2) the lateral boundaries of areas 36 and TF were placed more medially than in other studies, with concomitant expansion of the area TE; 3) the lateral boundary of area TF in *M. fuscata* was more laterally placed than that in *M. fascicularis* and *M. mulatta*, although there was no difference in architectonic structure; and 4) we recognized a caudal, granular part of the parahippocampal cortex that we termed "area TFO." This area closely resembles the laterally adjacent area TE and caudally adjacent area V4 and is clearly different from the more rostral area TF. We believe that our current findings have produced a more objective and reproducible description of these cortical areas in macaque monkeys. In the following sections, we discuss our findings along with the previous studies of these medial temporal lobe areas.

Comparison with previous architectonic studies of perirhinal cortex (areas 35 and 36)

Architectonic organization and boundaries of area 35. Although there is relatively good agreement on the general location and cytoarchitectonic organization of area 35, there are considerable differences between descriptions of its size and precise borders. Our definition of area 35 relies in part on the same cytoarchitectonic char-

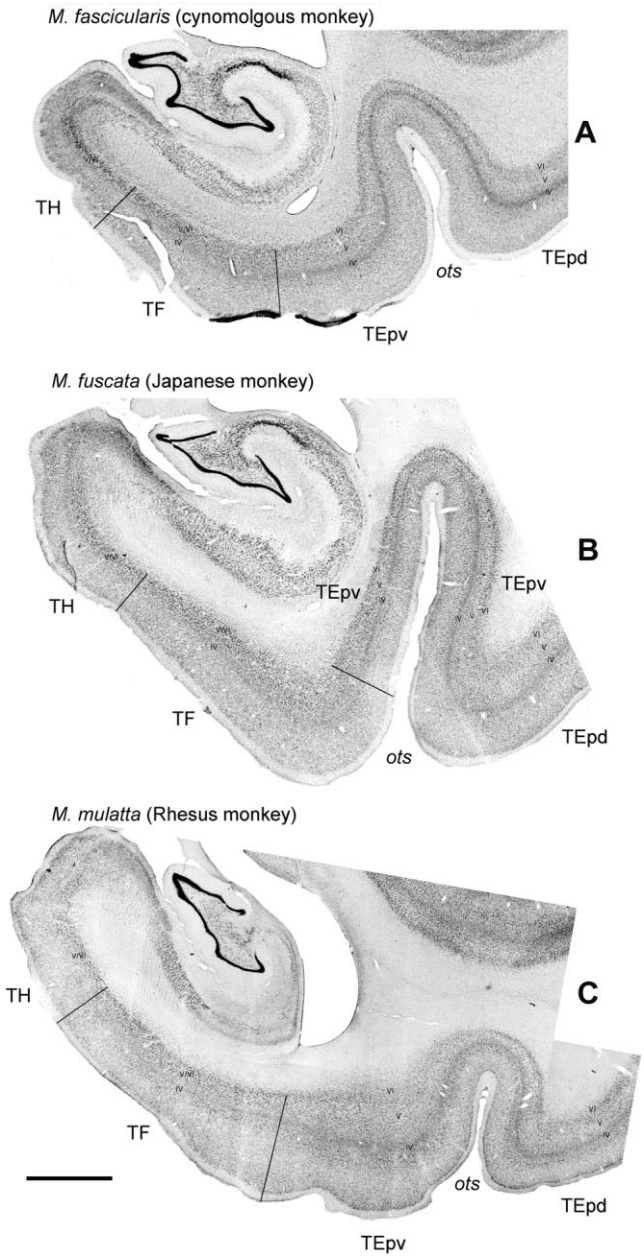

Fig. 20. Cytoarchitectonic organization and borders of area TF in three macaque species (**A–C**). Note that the border between TF and TEpv, as defined by the change from a relatively homogeneous pattern in layers IV, V, and VI to a trilaminar pattern, is on the medial bank of the ots in *M. fuscata* (B) but medial to the medial lip of the ots in *M. fascicularis* and *M. mulatta* (A,C). Scale bar = 2 mm.

acteristics reported by Van Hoesen and Pandya (1975a) and Amaral et al. (1987) from Nissl-stained sections, but we have also noted other chemoarchitectonic and laminar features with parvalbumin, SMI-32, and m2-AChR staining (Figs. 3, 4). Area 35a of Van Hoesen and Pandya (Van Hoesen and Pandya 1975a; see our Fig. 23D) and most of area 35 of Amaral et al. (1987) correspond to area 35 in the present study.

The boundary between the entorhinal cortex (area 28Ll) and area 35 in the lateral fundus of the rhinal sulcus is particularly obvious in sections stained for parvalbumin and m2-AChR (Figs. 3, 4). This agrees generally, if not precisely, with the location of the borders drawn from Nissl-stained sections by Van Hoesen and Pandya (1975a) between areas 35a and Pr2 (Fig. 23D) and by Amaral et al. (1987) between areas 35 and EL. The projection from presubiculum to the entorhinal cortex also extends to the same point at the lateral edge of the fundus of the rhinal sulcus, providing a connectional criterion for this boundary (Saunders and Rosene, 1988, their Fig. 13).

We set the rostral limit of area 35 at the rostral end of the rhinal sulcus. This differs from the delineation by Amaral and his colleagues (Insausti et al., 1987; Suzuki and Amaral, 2003; see also Munoz and Insausti, 2005), who extended area 35 rostrally and dorsally from the rhinal sulcus into the medial part of the temporal pole, overlapping the rostral part of the periamygdaloid cortex and even the piriform cortex. After the earlier description by Moran et al. (1987), we have recognized this region as a separate agranular temporal polar area (TGa; Kondo et al., 2003), which is clearly different than area 35 in Nissl-, parvalbumin-, and SMI-32-stained material. A striking finding is that the cell-sparse layer between layers III and V (layer "S"), which is prominent in area 35, was absent in area TGa. The strong parvalbumin staining seen in area 35 is also lacking in area TGa (see Fig. 2). In addition, area TGa is connected to both orbital and medial prefrontal networks, to both dorsal and ventral temporal pole (Kondo et al., 2003, Kondo et al., 2005), and to both superior and inferior temporal cortex (Saleem, Price, and Hashikawa, unpublished observations), whereas the perirhinal cortex is connected only to the orbital network, ventral temporal pole, and inferior temporal cortex (Kondo et al., 2005).

Architectonic organization and boundaries of area 36. There has been considerable variability in the description and delineation of the area 36, both between different investigators and in some cases even between different studies by the same investigator(s). In recent descriptions, Suzuki and Amaral (Suzuki and Amaral 1994a, Suzuki and Amaral 2003; see also Amaral et al., 1987; Insausti et al., 1987) described area 36 as a dysgranular cortex with aggregates of cells in layer II and darkly stained cells in deep layers (comparable to the description of area 35b by Van Hoesen and Pandya, 1975a). They extended area 36 laterally, however, to include most of the inferior temporal gyrus and rostrally to include substantial parts of the dorsal and ventral temporal pole (see also Munoz and Insausti, 2005). They also distinguished caudal and rostral subdivisions of area 36 (36c and 36r, respectively) and medial and lateral subdivisions in both of these subdivisions (36cm, 36cl, 36rm, 36rl; Suzuki and Amaral, 1994a, Suzuki and Amaral, 2003). Within the temporal pole, they recognized areas 36rm and 36rl in the ventromedial part and 36d in the dorsomedial part.

In the present study, we restricted area 36 to the lateral bank of the rhinal sulcus and the medial part of the inferior temporal gyrus, based on cytoarchitectonic and chemoarchitectonic observations. Although we distinguished three subdivisions within the rostrocaudal extent of area 36 (36c, 36r, and 36p), our subdivisions did not match closely with the rostrocaudal subdivisions of Suzuki and Amaral (Suzuki and Amaral 1994a, Suzuki and Amaral 2003). Our area 36p corresponds to the rostral part of their area 36r, whereas the border between our

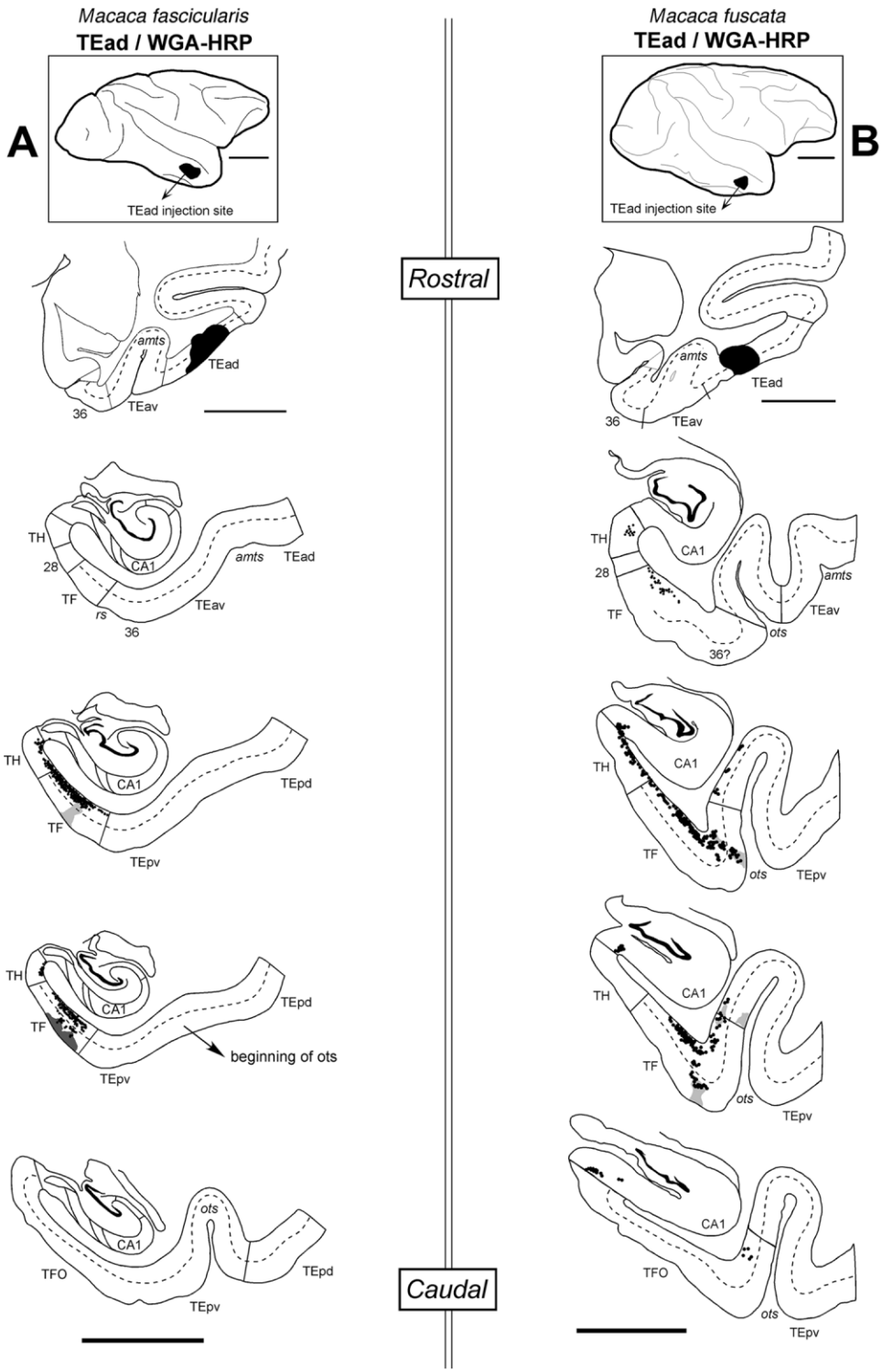

Fig. 21. Distribution of retrogradely labeled neurons (dots) and anterogradely labeled terminals (gray shading) in the parahippocampal cortex (areas TF and TH) following WGA-HRP injections into area TEad in cynomolgous monkey (*M. fascicularis*; **A**) and Japanese monkey (*M. fuscata*; **B**). Injections sites (black area) are shown on the lateral view of the brain at top and on the most rostral section. Note that the labeling is essentially limited to areas TF and TH in both species, with very little labeling in area TEpv. The boundary with area TEpv, determined by cytoarchitectonic criteria, is in the middle of the posterior parahippocampal gyrus in the cynomolgous monkey but is within the ots in the Japanese monkey. Scale bars = 5 mm; 10 mm in the inset on the top.

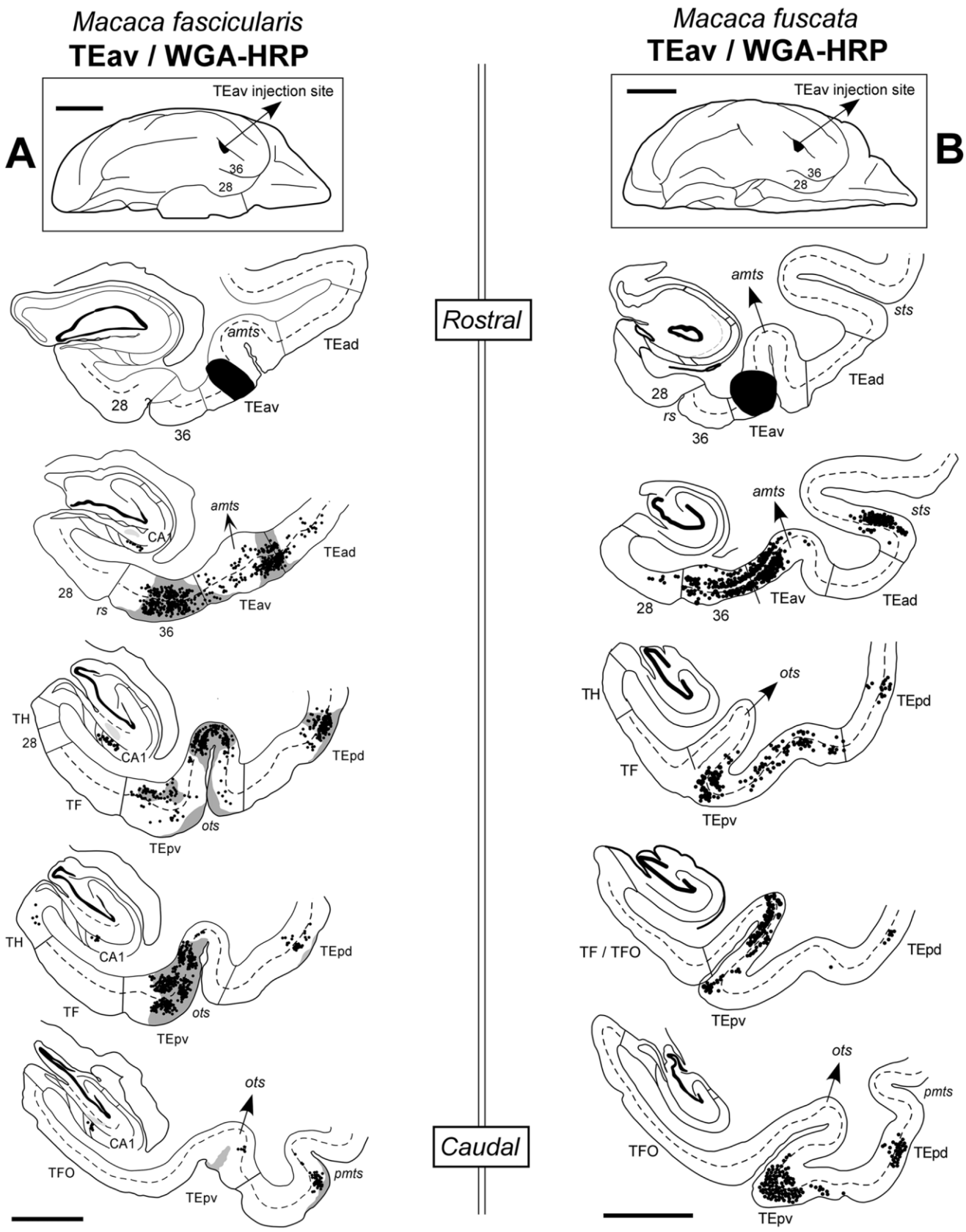

Fig. 22. Distribution of retrogradely labeled neurons (dots) and anterogradely labeled terminals (gray shading) in area TEpv following WGA-HRP injections into area TEav in cynomolgous monkey (*M. fascicularis*; **A**) and the Japanese monkey (*M. fuscata*; **B**). Injections sites (black area) are shown on the ventral view of the brain at top and on the first section. Anterogradely labeled terminals are not indicated in B. Note that, in both species, the label does not extend into area TF, defined by cytoarchitectonic criteria. In the cynomolgous monkey, however, the labeling extends onto the parahippocampal gyrus medial to the ots, whereas, in the Japanese monkey, the label is restricted to the lateral bank and lip of the ots. Scale bars = 3 mm in A; 5 mm in B; 10 mm in the inset on the top.

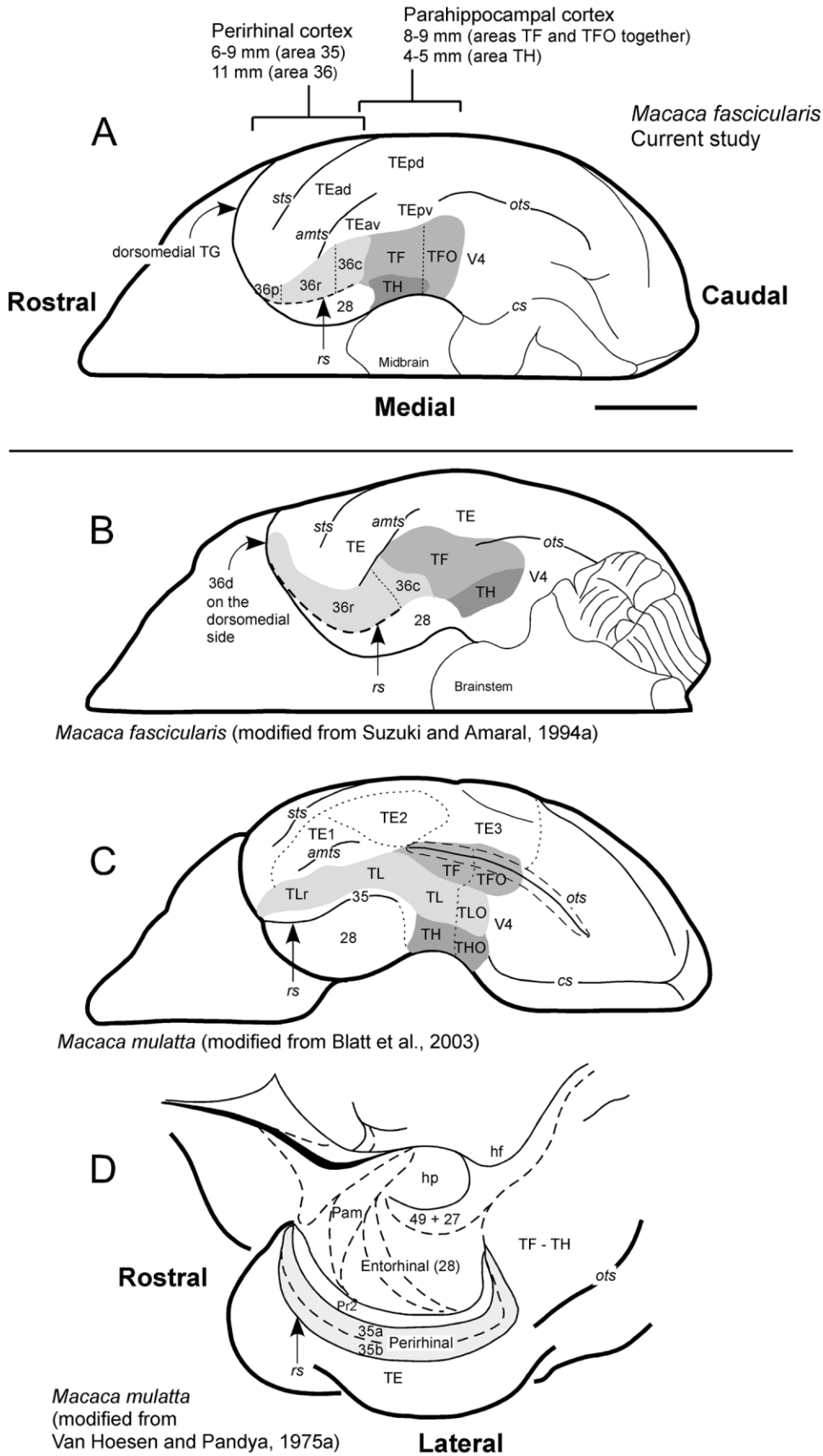

Fig. 23. Ventral view of the *M. fascicularis* brain (**A**), illustrating the spatial extent and subdivisions of the perirhinal cortex (areas 35 and 36), parahippocampal cortex (areas TF and TH), and surrounding regions (areas TE, 28, and V4) based on the current study. The numbers at top indicate the rostrocaudal extent of perirhinal and parahippocampal cortices, obtained from MRI images and a series of histology sections. For comparison, we provide the extent and subdivision of perirhinal and parahippocampal cortices in *M. fascicularis* or *M. mulatta*, as delineated in other studies (**B–D**). Note that our area 36 corresponds approximately to the rostral part of area TL of Blatt et al. (2003) and did not extend into the dorsomedial part of the temporal pole (36d of the Suzuki and Amaral, 1994a). Other important differences in our study include the position of the lateral border of areas 36 and TF and the recognition of area TFO (see Discussion). Scale bar = 10 mm.

areas 36r and 36c is more rostral than that of Suzuki and Amaral (2003). We did not recognize mediolateral subdivisions within area 36, primarily because the mediolateral extent of our area 36 was smaller. The major differences between our description and that of the Amaral group, however, are in the rostral and lateral borders of area 36 with the temporal pole areas and with area TE (see below).

In our delineation, the border between areas 36 and TEav was based primarily on the architectonic distinction among layers IV, V, and VI and on the greater density of layer IV in TE (Fig. 6). Based on these criteria, the boundary between areas 36 and TE is usually located midway between the amts and rhinal sulcus, such that only the medial part of the inferior temporal gyrus is included with area 36 (see Figs. 1C, 6). Although this definition of area 36 differs from that of Suzuki and Amaral (2003), it closely matches other descriptions/illustrations that were based on Nissl, immunocytochemical, or histochemical staining methods in Japanese monkeys (Saleem and Tanaka, 1996; Yukie, 2000) and cynomolgous monkeys (Amaral et al., 1987; Leonard et al., 1995, their Fig. 9).

Unfortunately, it is difficult to define area 36 clearly based on connections. Although it has been suggested that direct connections with hippocampus or entorhinal cortex can serve to define the perirhinal and parahippocampal cortices (Insausti et al., 1987; Suzuki and Amaral, 1990, Suzuki and Amaral, 1994a, Suzuki and Amaral, 2003), this criterion is not absolute. More lateral areas of the temporal cortex (areas TEad, TEav, TEpv, and the fundus of the STS), and even more distant cortex such as the parietal cortex (areas 7a and 7b) are connected directly with the hippocampus (Yukie and Iwai, 1988; Saleem and Hashikawa, 1998; Rockland and Van Hoesen, 1999; Yukie, 2000; Zhong and Rockland, 2004; Zhong et al., 2005; Ichinohe and Rockland, 2005b). Similarly, the origin of the projection to the entorhinal cortex extends laterally beyond area 36, to the medial lip of the amts (Saleem and Tanaka, 1996), including cortex that most investigators agree is part of area TE (Saleem and Tanaka, 1996; Yukie, 2000; Naya et al., 2003; Yoshida et al., 2003; Zhong and Rockland, 2003; Ichinohe and Rockland, 2005b).

Is the dorsal temporal pole part of the perirhinal cortex? Although the dorsomedial aspect of the temporal pole has been included in area 36 in some descriptions (Insausti et al., 1987; Suzuki and Amaral, 1994a, Suzuki and Amaral, 2003; Lavenex et al., 2002, Lavenex et al., 2004; Munoz and Insausti, 2005; Mohedano-Moriano et al., 2005), there are substantial architectonic differences between this region and other parts of area 36 (Figs. 8, 9). In addition, the connections of the dorsomedial temporal pole with the prefrontal and other temporal cortical areas are substantially different from those of the perirhinal cortex (Kondo et al., 2003, Kondo et al., 2005). The dorsomedial temporal pole is reciprocally connected with medial network areas in the prefrontal cortex, the rostral superior temporal gyrus (STGr), the entorhinal cortex, and the parahippocampal gyrus (Kondo et al., 2003; see also Moran et al., 1987); the strongest connections are with the STGr. We also found a similar pattern of connections after retrograde and anterograde tracer injections into the STGr (Saleem and Price, 2005). In contrast, perirhinal cortex is connected with the ventromedial temporal pole and with the orbital network areas in the prefrontal cortex, the visual association area TEav (the strongest connection), and the ventral bank and fundus of the superior temporal sulcus (Saleem and Tanaka, 1996; Saleem et al., 2000; Kondo et al., 2003, Kondo et al., 2005). Suzuki and Amaral (1994a) also indicate that the connections of their area 36d are distinct from those of other subregions of the perirhinal cortex (e.g., their areas 36r and 36c). Strikingly, even the intrinsic connections within the temporal pole are largely restricted to either the dorsal or the ventral regions, with very few connections from dorsal to ventral or vice versa (Kondo et al., 2003).

Thus the current architectonic data together with the previous architectonic or/and connectional data (Moran et al., 1987; Saleem and Tanaka, 1996; Kondo et al., 2003) argue against the view that the dorsomedial temporal pole is part of the perirhinal cortex (Insausti et al., 1987; Suzuki and Amaral, 1994a, Suzuki and Amaral, 2003; Lavenex et al., 2002, Lavenex et al., 2004; Munoz and Insausti, 2005; Mohedano-Moriano et al., 2005). Instead, it would appear that the dorsal temporal pole is related to a cortical system that connects the STGr, the medial prefrontal network, and the parahippocampal cortex. This system is largely independent of the ventral temporal pole and perirhinal cortex, which are related more to area TE and the orbital prefrontal network (Price, 2005; see his Fig. 7).

Comparison with previous architectonic studies of parahippocampal cortex (areas TF and TH)

Architectonic organization and boundaries of areas TF and TH. In their original description from monkeys, von Bonin and Bailey (von Bonin and Bailey 1947, their Figs. 18–21) distinguished areas TF and TH on the medial side of the occipitotemporal sulcus (ots) and area TE lateral to the ots. As in other parts of the cortex, they did not indicate clear boundaries between these areas. With the demonstration of specific connections, there have been attempts to define these architectonic boundaries precisely, although there are substantial differences in descriptions. In recent descriptions, Blatt et al. (2003) recognized three areas, TH, TL, and TF, with area TL extending from the rostral end of the rhinal sulcus (replacing area 36) to visual area 19 (V4). Suzuki and Amaral (2003) referred only to TH and TF, although they subdivided area TF into medial and lateral subregions (TFm and TFl, respectively). Their area TFl extends up to the medial lip of the ots; rostrally, it extends lateral to the caudal part of area 36.

We have restricted areas TF/TH to the rostral and medial part of the posterior parahippocampal gyrus based on the cytoarchitectonic and chemoarchitectonic observations and on previous data on the connections with the medial prefrontal network and related areas such as the dorsal temporal pole (Kondo et al., 2005). As shown in this paper, this definition of area TF is also supported by connections with areas TEad and TEav (Figs. 21, 22). The lateral boundary of our area TF is therefore more medial than that in other descriptions, with concomitant expansion of area TEpv.

Our area TF corresponds approximately to TFm and part of area TFl of Suzuki and Amaral (2003) and to the caudal part of area TL of Blatt et al. (2003). It does not include most of area TFl of Suzuki and Amaral (2003), or area TF of Blatt et al. (2003), which we consider to be part of area TEpv (Fig. 16). Our area TF also does not include

the more rostral part of Suzuki and Amaral's (Suzuki and Amaral 1994a, Suzuki and Amaral, 2003) area TF, which extended lateral to the perirhinal cortex and medial to the anterior middle temporal sulcus. We consider this region to be part of area TEav (Fig. 6; see the perirhinal section). Finally, our parahippocampal cortex does not include the rostral part of area TL described by Blatt et al. (2003); this region corresponds approximately to area 36 described in the current study.

The caudal part of the parahippocampal cortex described by both Suzuki and Amaral (2003) and Blatt et al. (2003) is substantially more granular than the rostral part. This region resembles area TEpv and/or area V4 more than it does area TF, as we have described it in this paper. We have termed this caudal subregion "area TFO," following a terminology similar to that used by Blatt et al. (2003). Our TFO corresponds to both THO and TLO of Blatt et al. (2003), but it does not include more lateral area that they labeled TFO, which we consider part of area TEpv (Fig. 23, compare A and C).

Area TFO would also appear to correspond to an area that Boussaoud et al. (1991) referred to as a "visually responsive zone within TF" (VTF). They found evidence for at least a coarse retinotopy, with the fovea represented laterally and the peripheral retina more medially. They did not find visually responsive cells more anteriorly in area TF itself. It is uncertain whether area TFO should be considered part of the parahippocampal cortex or part of the visual association cortex.

Organization of perirhinal and parahippocampal cortices in different species of macaques

Although it is generally assumed that the anatomical and functional organization of different cortical areas is similar in different macaque monkeys, there are several cases in which specific areas vary in size and shape across monkey species. For example, striking differences in the size and relative positions of the central and surrounding auditory fields were reported between *M. fuscata* and *M. fascicularis* (Jones et al., 1995). A more subtle difference in the cytoarchitectonic organization of the entorhinal cortex (area 28) has also been distinguished between *M. fascicularis* and *M. mulatta* (Van Hoesen and Pandya, 1975a; Amaral et al., 1987).

We found that the location and cytoarchitectonic features of the perirhinal cortex, and its border with area TE, were generally similar in all three species of macaques (*M. fascicularis*, *M. fuscata*, and *M. mulatta*; Figs. 10, 11). In contrast, the lateral boundary of the parahippocampal cortex (area TF) with posteroventral area TE (TEpv) was different in *M. fuscata* from the other two species, although the architectonic organization of this cortex was similar in all three species of macaques. That is, the transition from areas TEpv to TF, based on both cytoarchitectonic criteria and connections, is in the medial bank of the ots in *M. fuscata*, but about 3 mm medial to the ots in *M. fascicularis* and *M. mulatta*. It is possible that some of this apparent difference in position of the border between TF and TEpv is due to a difference in the ots, which is generally much deeper in *M. fuscata* than in the other two species. However, in some *M. fascicularis* individuals, the ots is also very deep, but the boundary between TF and TEpv is still found about 2 mm medial to the ots.

The perirhinal/parahippocampal region has also been described for baboons (Blaizot et al., 2004). This description, which is based only on Nissl-stained sections, applies the earlier delineation in macaques by Amaral et al. (1987) and Suzuki and Amaral (Suzuki and Amaral, 1994a, Suzuki and Amaral, 2003) to baboons. Because of this, the current description in this paper has the same differences from and similarities to the one in baboons as it does to the descriptions in macaques. It is worth noting that the boundary between areas TF and TE in baboons is shown at the medial lip of the ots (Blaizot et al., 2004). Based on the dark-light-dark pattern in layers IV, V, and VI in area TE, which is apparent in the baboon sections shown in their Figure 2 (sections 12 and 13), we would place this border still more medially (see description of TE/TF border in Results). In either case, the boundary in baboons is similar to that in *M. fascicularis* and *M. mulatta* and different from that in *M. fuscata*.

Human parahippocampal region: where is the parahippocampal place area (PPA)? Does it correspond to monkey parahippocampal cortex?

The position of the parahippocampal cortex in humans does not appear to have been well studied architectonically since Von Economo and Koskinas (1925) originally defined areas TF and TH. Area TF, as outlined in humans by Von Economo and Koskinas (1925), is a relatively large area that includes the posterior two-thirds of the parahippocampal gyrus. It corresponds approximately to the caudal part of Brodmann's area 36 (1909). There is no recent detailed description of the parahippocampal cortex in humans, although Vogt et al. (2001) described the architectonic areas around the splenium of the corpus callosum, including the parahippocampal cortex. They referred to the parahippocampal areas as the caudal part of area 36 (areas 36′v and 36′d).

Functional imaging methods have identified a "parahippocampal place area" (PPA) in the posterior parahippocampal gyrus or the adjacent fusiform gyrus, which is specifically activated by images depicting places (Aguirre et al., 1998; Epstein et al., 1999; Ishai et al., 1999). Such a function fits well with the proposed role of the parahippocampal cortex in spatial memory (see above), and the position of the PPA fits generally with the posterior parahippocampal cortex.

The position of the PPA varies somewhat among studies, however, and from left to right in the same study (Aguirre et al., 1998; Epstein et al., 1999; Ishai et al., 1999; Spiridon et al, 2006). As shown in the present paper, there are five or six architectonic areas in the posterior parahippocampal region of the macaque monkey, and it is not clear whether the PPA corresponds to one or several of them. Most illustrations of functional activity locate the PPA at a relatively lateral and caudal level, overlapping the collateral sulcus at or behind the splenium of the corpus callosum (Epstein and Kanwisher, 1998; Ishai et al., 1999). Further cytoarchitectonic analysis of the human posterior parahippocampal gyrus is clearly needed, but it is possible that the PPA corresponds more closely to area TFO, and possibly to ventral area V4, than to area TF, as defined in this study.

ACKNOWLEDGMENTS

We thank Tsukuba Primate Center for providing the *Macaca fascicularis* monkeys and for surgical assistance and A.H. Asiyabegum for surgical and histological assistance. We also thank Drs. K.S. Rockland and N. Ichinohe (Riken Brain Science Institute) for help with the MAP-analyzer program.

LITERATURE CITED

Aguirre GK, Zarahn E, D'Esposito M. 1998. An area within human ventral cortex sensitive to building stimuli: evidence and implications. Neuron 21:373–383.

Alvarado MC, Bachevalier J. 2005. Comparison of the effects of damage to the perirhinal and parahippocampal cortex on transverse patterning and location memory in rhesus macaques. J Neurosci 25:1599–1609.

Amaral DG, Insausti R, Cowan WM. 1987. The entorhinal cortex of the monkey: I. Cytoarchitectonic organization. J Comp Neurol 264:326–355.

Baxter MG, Murray EA. 2001. Opposite relationship of hippocampal and rhinal cortex damage to delayed nonmatching-to-sample deficits in monkeys. Hippocampus 11:61–71.

Blaizot X, Martinez-Marcos A, Arroyo-Jimenez M, Marcos P, Artacho-Perula E, Munoz M, Chavoix C, Insausti R. 2004. The parahippocampal gyrus in the baboon: anatomical, cytoarchitectonic and magnetic resonance imaging (MRI) studies. Cereb Cortex 14:231–246.

Blatt GJ, Rosene DL. 1998. Organization of direct hippocampal efferent projections to the cerebral cortex of the rhesus monkey: projections from CA1, prosubiculum, and subiculum to the temporal lobe. J Comp Neurol 392:92–114.

Blatt GJ, Pandya DN, Rosene DL. 2003. Parcellation of cortical afferents to three distinct sectors in the parahippocampal gyrus of the rhesus monkey: an anatomical and neurophysiological study. J Comp Neurol 466:161–179.

Boussaoud D, Desimone R, Ungerleider LG. 1991. Visual topography of area TEO in the macaque. J Comp Neurol 306:554–575.

Brodmann K. 1909. Vergleichende Lokalisationslehre der Grosshirnrinde. Leipzig: Johann Ambrosius Barth.

Buckley MJ, Gaffan D. 1997. Impairment of visual object-discrimination learning after perirhinal cortex ablation. Behav Neurosci 111:467–75.

Buckley MJ, Gaffan D, Murray EA. 1997. Functional double dissociation between two inferior temporal cortical areas: perirhinal cortex versus middle temporal gyrus. J Neurophysiol 77:587–98.

Campbell MJ, Morrison JH. 1989. Monoclonal antibody to neurofilament protein (SMI-32) labels a subpopulation of pyramidal neurons in the human and monkey neocortex. J Comp Neurol 282:191–205.

Carmichael ST, Price JL. 1994. Architectonic subdivision of the orbital and medial prefrontal cortex in the macaque monkey. J Comp Neurol 346:366–402.

Carmichael ST, Clugnet MC, Price JL. 1994. Central olfactory connections in the macaque monkey. J Comp Neurol 346:403–434.

Cheng K, Saleem KS, Tanaka K. 1997. Organization of corticostriatal and corticoamygdalar projections arising from the anterior inferotemporal area TE of the macaque monkey: a *Phaseolus vulgaris* leucoagglutinin study. J Neurosci 17:7902–7925.

Epstein R, Kanwisher N. 1998. A cortical representation of the local visual environment. Nature 392:598–601.

Epstein R, Harris A, Stanley D, Kanwisher N. 1999. The parahippocampal place area: recognition, navigation, or encoding? Neuron 23:115–125.

Flynn DD, Mash DC. 1993. Distinct kinetic binding properties of N-[^{3}H]-methylscopolamine afford differential labeling and localization of M1, M2, and M3 muscarinic receptor subtypes in primate brain. Synapse 14:283–296.

Gaffan D, Murray EA. 1992. Monkeys (*Macaca fascicularis*) with rhinal cortex ablations succeed in object discrimination learning despite 24-hour intertrial intervals and fail at matching to sample despite double sample presentations. Behav Neurosci 106:30–38.

Garey LJ. 1994. Brodmann's "Localization in the cerebral cortex." London: Smith-Gordon.

Gibson AR, Hansma DI, Houk JC, Robinson FR. 1984. A sensitive low artifact TMB procedure for the demonstration of WGA-HRP in the CNS. Brain Res 298:235–241.

Goldstein ME, Sternberger LA, Sternberger NH. 1987. Varying degrees of phosphorylation determine microheterogeneity of the heavy neurofilament polypeptide (Nf-H). J Neuroimmunol 14:135–148.

Gower EC. 1989. Efferent projections from limbic cortex of the temporal pole to the magnocellular medial dorsal nucleus in the rhesus monkey. J Comp Neurol 280:343–358.

Hackett TA, Stepniewska I, Kaas JH. 1998. Subdivisions of auditory cortex and ipsilateral cortical connections of the parabelt auditory cortex in macaque monkeys. J Comp Neurol 394:475–495.

Hadfield WS, Baxter MG, Murray EA. 2003. Effects of combined and separate removals of rostral dorsal superior temporal sulcus cortex and perirhinal cortex on visual recognition memory in rhesus monkeys. J Neurophysiol 90:2419–2427.

Hof PR, Morrison JH. 1995. Neurofilament protein defines regional patterns of cortical organization in the macaque monkey visual system: a quantitative immunohistochemical analysis. J Comp Neurol 352:161–186.

Ichinohe N, Rockland KS. 2005a. Distribution of synaptic zinc in the macaque monkey amygdala. J Comp Neurol 489:135–147.

Ichinohe N, Rockland KS. 2005b. Zinc-enriched amygdalo- and hippocampo-cortical connections to the inferotemporal cortices in macaque monkey. Neurosci Res 53:57–68.

Insausti R, Amaral DG, Cowan WM. 1987. The entorhinal cortex of the monkey: II. Cortical afferents. J Comp Neurol 264:356–395.

Ishai A, Ungerleider LG, Martin A, Schouten JL, Haxby JV. 1999. Distributed representation of objects in the human ventral visual pathway. Proc Natl Acad Sci U S A 96:9379–9384.

Jones EG, Dell'Anna ME, Molinari M, Rausell E, Hashikawa T. 1995. Subdivisions of macaque monkey auditory cortex revealed by calcium-binding protein immunoreactivity. J Comp Neurol 362:153–170.

Kondo H, Saleem KS, Price JL. 2003. Differential connections of the temporal pole with the orbital and medial prefrontal networks in macaque monkeys. J Comp Neurol 465:499–523.

Kondo H, Saleem KS, Price JL. 2005. Differential connections of the perirhinal and parahippocampal cortex with the orbital and medial prefrontal networks in macaque monkeys. J Comp Neurol 493:479–509.

Lavenex P, Suzuki WA, Amaral DG. 2002. Perirhinal and parahippocampal cortices of the macaque monkey: projections to the neocortex. J Comp Neurol 447:394–420.

Lavenex P, Suzuki WA, Amaral DG. 2004. Perirhinal and parahippocampal cortices of the macaque monkey: intrinsic projections and interconnections. J Comp Neurol 472:371–394.

Leonard BW, Amaral DG, Squire LR, Zola-Morgan S. 1995. Transient memory impairment in monkeys with bilateral lesions of the entorhinal cortex. J Neurosci 15:5637–5659.

Levey AI, Kitt CA, Simonds WF, Price DL, Brann MR. 1991. Identification and localization of muscarinic acetylcholine receptor proteins in brain with subtype-specific antibodies. J Neurosci 11:3218–3226.

Levey AI, Edmunds SM, Hersch SM, Wiley RG, Heilman CJ. 1995. Light and electron microscopic study of m2 muscarinic acetylcholine receptor in the basal forebrain of the rat. J Comp Neurol 351:339–356.

Malkova L, Mishkin M. 2003. One-trial memory for object-place associations after separate lesions of hippocampus and posterior parahippocampal region in the monkey. J Neurosci 23:1956–1965.

Markowitsch HJ, Emmans D, Irle E, Streicher M, Preilowski B. 1985. Cortical and subcortical afferent connections of the primate's temporal pole: a study of rhesus monkeys, squirrel monkeys, and marmosets. J Comp Neurol 242:425–458.

Martin-Elkins CL, Horel JA. 1992. Cortical afferents to behaviorally defined regions of the inferior temporal and parahippocampal gyri as demonstrated by WGA-HRP. J Comp Neurol 321:177–192.

Mash DC, White WF, Mesulam MM. 1988. Distribution of muscarinic receptor subtypes within architectonic subregions of the primate cerebral cortex. J Comp Neurol 278:265–274.

Meunier M, Bachevalier J, Mishkin M, Murray EA. 1993. Effects on visual recognition of combined and separate ablations of the entorhinal and perirhinal cortex in rhesus monkeys. J Neurosci 13:5418–5432.

Mohedano-Moriano A, Martinez-Marcos A, Munoz M, Arroyo-Jimenez MM, Marcos P, Artacho-Perula E, Blaizot X, Insausti R. 2005. Reciprocal connections between olfactory structures and the cortex of the rostral superior temporal sulcus in the *Macaca fascicularis* monkey. Eur J Neurosci 22:2503–2518.

Moran MA, Mufson EJ, Mesulam M-M. 1987. Neural inputs into the temporopolar cortex of the rhesus monkey. J Comp Neurol 256:88–103.

Munoz M, Insausti R. 2005. Cortical efferents of the entorhinal cortex and the adjacent parahippocampal region in the monkey (*Macaca fascicularis*). Eur J Neurosci 22:1368–1388.

Murray EA, Bussey TJ. 1999. Perceptual-mnemonic functions of the perirhinal cortex. Trends Cogn Sci 3:142–151.

Murray EA, Richmond BJ. 2001. Role of perirhinal cortex in object perception, memory, and associations. Curr Opin Neurobiol 11:188–193.

Naya Y, Yoshida M, Miyashita Y. 2003. Forward processing of long-term associative memory in monkey inferotemporal cortex. J Neurosci 23: 2861–2871.

Pitkanen A, Amaral DG. 1991. Demonstration of projections from the lateral nucleus to the basal nucleus of the amygdala: a PHA-L study in the monkey. Exp Brain Res 83:465–470.

Pitkanen A, Amaral DG. 1993. Distribution of parvalbumin-immunoreactive cells and fibers in the monkey temporal lobe: the hippocampal formation. J Comp Neurol 331:37–74.

Price JL. 2005. Free will vs. survival: brain systems that underlie intrinsic constraints on behavior. J Comp Neurol 493:132–139.

Rockland KS, Van Hoesen GW. 1999. Some temporal and parietal cortical connections converge in CA1 of the primate hippocampus. Cereb Cortex 9:232–237.

Saleem KS, Hashikawa T. 1998. Connections of anterior inferotemporal area TE and perirhinal cortex with hippocampal formation in the macaque monkey. Soc Neurosci Abstr 24:898.

Saleem KS, Price J. 2005. Distinct complementary circuits link medial and orbital prefrontal networks with specific temporal and other cortical areas in macaque monkey. Soc Neurosci Abstr 35:854.5.

Saleem KS, Tanaka K. 1996. Divergent projections from the anterior inferotemporal area TE to the perirhinal and entorhinal cortices in the macaque monkey. J Neurosci 16:4757–4775.

Saleem KS, Suzuki W, Tanaka K, Hashikawa T. 2000. Connections between anterior inferotemporal cortex and superior temporal sulcus regions in the macaque monkey. J Neurosci 20:5083–5101.

Saunders RC, Rosene DL. 1988. A comparison of the efferents of the amygdala and the hippocampal formation in the rhesus monkey: I. Convergence in the entorhinal, prorhinal, and perirhinal cortices. J Comp Neurol 271:153–184.

Saunders RC, Rosene DL, Van Hoesen GW. 1988. Comparison of the efferents of the amygdala and the hippocampal formation in the rhesus monkey: II. Reciprocal and non-reciprocal connections. J Comp Neurol 271:185–207.

Seltzer B, Pandya DN. 1976. Some cortical projections to the parahippocampal area in the rhesus monkey. Exp Neurol 50:146–160.

Seltzer B, Pandya DN. 1989. Frontal lobe connections of the superior temporal sulcus in the rhesus monkey. J Comp Neurol 281:97–113.

Spiridon M, Fischl B, Kanwisher N. 2006. Location and spatial profile of category-specific regions in human extrastriate cortex. Hum Brain Mapping 27:77–89.

Stefanacci L, Suzuki WA, Amaral DG. 1996. Organization of connections between the amygdaloid complex and the perirhinal and parahippocampal cortices in macaque monkeys. J Comp Neurol 375:552–582.

Sternberger LA, Sternberger NH. 1983. Monoclonal antibodies distinguish phosphorylated and non-phosphorylated forms of neurofilaments in situ. Proc Natl Acad Sci U S A 80:6126–6130.

Suzuki WA, Amaral DG. 1990. Cortical inputs to the CA1 field of the monkey hippocampus originate from the perirhinal and parahippocampal cortex but not from area TE. Neurosci Lett 115:43–48.

Suzuki WA, Amaral DG. 1994a. Perirhinal and parahippocampal cortices of the macaque monkey: cortical afferents. J Comp Neurol 350:497–533.

Suzuki WA, Amaral DG. 1994b. Topographic organization of the reciprocal connections between the monkey entorhinal cortex and the perirhinal and parahippocampal cortices. J Neurosci 14:1856–1877.

Suzuki WA, Amaral DG. 2003. Perirhinal and parahippocampal cortices of the macaque monkey: cytoarchitectonic and chemoarchitectonic organization. J Comp Neurol 463:67–91.

Suzuki WA, Zola-Morgan S, Squire LR, Amaral DG. 1993. Lesions of the perirhinal and parahippocampal cortices in the monkey produce long-lasting memory impairment in the visual and tactual modalities. J Neurosci 13:2430–2451.

Van Hoesen GW. 1982. The parahippocampal gyrus: New observations regarding its cortical connections in the monkey. TINS 5:345–350.

Van Hoesen GW, Pandya DN. 1975a. Some connections of the entorhinal (area 28) and perirhinal (area 35) cortices of the rhesus monkey. I. Temporal lobe afferents. Brain Res 95:1–24.

Van Hoesen GW, Pandya DN. 1975b. Some connections of the entorhinal (area 28) and perirhinal (area 35) cortices of the rhesus monkey. III. Efferent connections. Brain Res 95:39–59.

Van Hoesen G, Pandya DN, Butters N. 1975. Some connections of the entorhinal (area 28) and perirhinal (area 35) cortices of the rhesus monkey. II. Frontal lobe afferents. Brain Res 95:25–38.

Vogt BA, Vogt LJ, Perl DP, Hof PR. 2001. Cytology of human caudomedial cingulate, retrosplenial, and caudal parahippocampal cortices. J Comp Neurol 438:353–376.

von Bonin G, Bailey P. 1947. The neocortex of *Macaca mulatta*. Urbana, IL: University of Illinois Press.

Von Economo C, Koskinas GN. 1925. Die Cytoarchitecktonik der Grosshirnrinde des erwachsenen Menschen. Berlin: Springer.

Witter MP, Amaral DG. 1991. Entorhinal cortex of the monkey: V. Projections to the dentate gyrus, hippocampus, and subicular complex. J Comp Neurol 307:437–459.

Witter MP, Van Hoesen GW, Amaral DG. 1989. Topographical organization of the entorhinal projection to the dentate gyrus of the monkey. J Neurosci 9:216–228.

Yoshida M, Naya Y, Miyashita Y. 2003. Anatomical organization of forward fiber projections from area TE to perirhinal neurons representing visual long-term memory in monkeys. Proc Natl Acad Sci U S A 100: 4257–4262.

Yukie M. 2000. Connections between the medial temporal cortex and the CA1 subfield of the hippocampal formation in the Japanese monkey (*Macaca fuscata*). J Comp Neurol 423:282–298.

Yukie M, Iwai E. 1988. Direct projections from the ventral TE area of the inferotemporal cortex to hippocampal field CA1 in the monkey. Neurosci Lett 88:6–10.

Yukie M, Takeuchi H, Hasegawa Y, Iwai E. 1990. Differential connectivity of inferotemporal area TE with the amygdala and the hippocampus in the monkey. In: Iwai E, Mishkin M, editors. Vision, memory, and the temporal lobe. New York: Elsevier. p 129–135.

Zhong YM, Rockland KS. 2003. Inferior parietal lobule projections to anterior inferotemporal cortex (area TE) in macaque monkey. Cereb Cortex 13:527–540.

Zhong YM, Rockland KS. 2004. Connections between the anterior inferotemporal cortex (area TE) and CA1 of the hippocampus in monkey. Exp Brain Res 155:311–119.

Zhong YM, Yukie M, Rockland KS. 2005. Direct projections from CA1 to the superior temporal sulcus in the monkey, revealed by single axon analysis. Brain Res 1035:211–114.

Zola-Morgan S, Squire LR, Amaral DG, Suzuki WA. 1989. Lesions of perirhinal and parahippocampal cortex that spare the amygdala and hippocampal formation produces severe memory impairment. J Neurosci 9:4355–4370.